NTNU – Trondheim
Norwegian University of
Science and Technology

Initial stages of metal dusting corrosion

Jihye Hwang

Abstract

Metal dusting is a disintegration phenomenon of metals and alloys into fine, dust-like particles. Metal dusting can be found in different reforming units in the petrochemical industry. As well as in reforming units, it can be found at high-temperature fuel cells.

The metal dusting corrosion phenomenon is initiated by unwanted carbon formation on the inner surface of process equipment. It occurs under a synthesis gaseous atmosphere (carbon activity >> 1) at high temperature with low oxygen/steam partial pressure. Since the gas contains carbon monoxide and hydrogen at high temperature, carbon is formed by CO reduction reaction and Boudouard reaction.

Carbon formation is kinetically controlled which means it is influenced by the catalytic properties and the local conditions like temperature and partial pressure. An oxide layer formed on the surface of alloys is protecting the alloy matrix from corrosion. Thickness of this oxide layer should be moderate. If the oxide layer is too thick, the metal alloys will have problems with thermal expansion and heat transfer. If it is too thin, however, the metal alloys cannot be protected from the corrosion.

To find the effects of oxidation temperature, CO exposure temperature and CO exposure time on carbon formation, oxidation treatments and CO exposure treatments were conducted. Samples were oxidized with 10% steam-Ar gas for 6 h at 540 °C or 760 °C. Subsequently, samples were exposed to 10% CO-Ar gas at 1 bar at 650 °C or 750 °C. Length of exposure time was different for each sample from 1 h to 20 h. After the experiments, surface of metal alloys was characterized by optical microscopy and scanning electron microscopy.

As a result of all experiments, the effect of CO exposure time can be summarized as follows. Regardless of sample exposure conditions, all samples have more carbon when they are exposed to CO gas for longer time. The effect of pre-treatment temperature is that lower temperature forms more carbon filaments. Finally, the effect of CO exposure treatment temperature is that lower temperature (650 °C) forms more carbon filaments than higher temperature (750 °C).

Preface

This thesis is written as a completion of the MSc. program in Chemical Engineering at the Norwegian University of Science and Technology, Department of Chemical Engineering. The thesis was written during spring semester 2015, and it accounts for 30 credits.

Writing this thesis has been an interesting and challenging task which has given me a good academic knowledge within this topic area.

I would like to thank Professor Hilde J. Venvik and P.V. Daham S. Gunawardana for a good guidance. Also, I want to give my special thanks to my parents.

I declare that this is an independent work according to the exam regulations of the Norwegian University of Science and Technology (NTNU).

Trondheim, June 2015

Jihye Hwang

Contents

List of figures

ix

List of tables

x

Abbreviations

*	Vacant site on the surface
ΔH°_{298}	Enthalpy change of a reaction at standard state (*i.e.* 25 °C and 1 atm)
ΔH	Enthalpy change of a reaction
A	Area
$A*$	Adsorbed species on the surface
a_c	Carbon activity
a_{c_i}	Carbon activity of reaction i
k_1	Rate constant of metal wastage
k_2	Rate constant of carbon deposition
k_3	Rate coefficient
K_i	Equilibrium constant of a reaction
m_C	Mass of carbon deposition
MCFC	Molten carbonate fuel cell
Me	Metal particle, especially Fe and Ni
MeO	Metal oxide
m_M	Mass of alloy converted into the corrosion product
P	Pressure gauge / pressure detector
P_i	Partial pressure of gas component i
r_C	Carbon deposition rate
RDS	Rate determining steps
r_M	Metal wastage rate
SE	Secondary electrons
SEM	Scanning electron microscopy
SOFC	Solid oxide fuel cell
T	Reaction temperature
T	Thermo couple / temperature detector
t	time

1. Introduction

1.1 Introduction of metal dusting

Metal dusting is a corrosion phenomenon which is a disintegration of metals and alloys into fine, dust-like particles. This phenomenon occurs under carburizing gas atmosphere having high carbon formation potential at high temperature with low oxygen/steam partial pressure. It is initiated by unwanted carbon formation on the inner surface of process equipment.

Metal dusting have been commonly observed in petrochemical production plants, coal gasification plants, natural gas processing, heat-treating and direct iron ore reduction [1, 2]. Metal dusting corrosion is also possible to be found at high-temperature fuel cells *i.e.* solid oxide fuel cell (SOFC) and molten carbonate fuel cell (MCFC) [3]. In synthesis gas production, the heat transfer and recovery sections after the reformer units are where the metal dusting mainly takes place. This is because of thermodynamics and kinetics of metal dusting. When the gas stream is passing through reforming units, it undergoes a temperature drop and eventually it reaches the temperature range from 400 °C to 800 °C, which metal dusting corrosion occurs. **Figure 1.1** shows the possibility of metal dusting in various types of reforming units in different petrochemical plants [4].

Metal dusting causes pits and holes on high alloy steels, general metal wastage on low alloy steels respectively [5]. Carbon (coke) with metal particles grows out from the metal surface as a result of metal dusting. The coke powder is easily carried away by the gases flowing at the high velocity in the industrial facilities, but the outgrowing protrusion form of coke powder is observed in laboratory scale [6]. **Figure 1.2** shows metal dusting corrosion attack on the super heater tube bundle at Statoil Tjeldbergodden methanol plant [7, 8].

Control of metal dusting corrosion is an important issue since it saves significant amount of cost for process unit replacement. The US Department of Energy (DOE) has reported that annually 220-290 million dollars could be saved in hydrogen production alone if the metal dusting is circumvented [9].
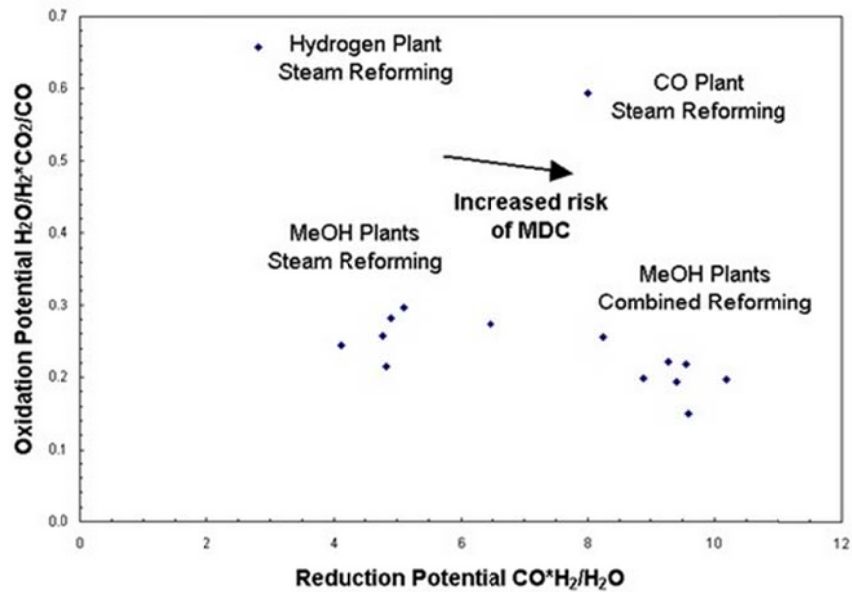
Figure 1.1 Possibility of metal dusting corrosion [4].
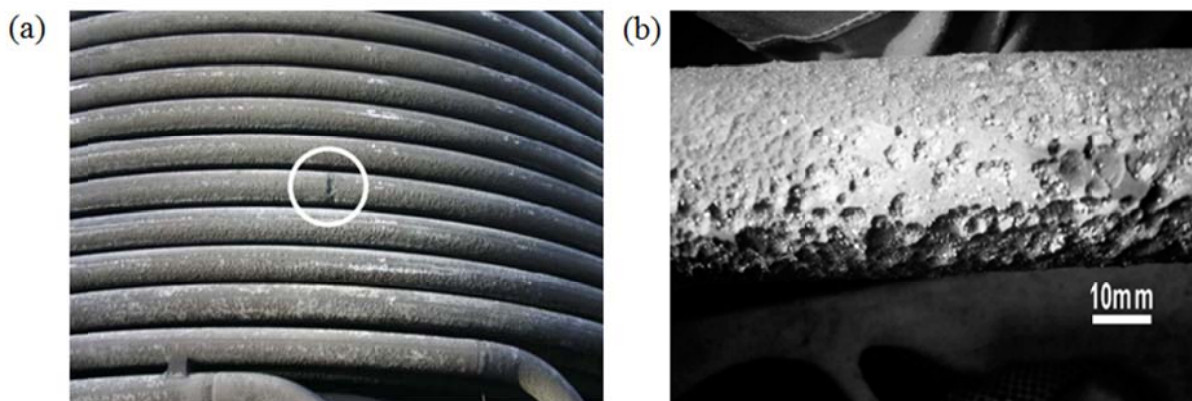
Figure 1.2 Metal dusting corrosion at Statoil Tjeldbergodden methanol plant: (a) super heater tube bundle [7]; (b) close-up [8].

2

1.2 Scope of the present work

Metal dusting corrosion was first found in 1945 by E. Camp and co-workers [3] and the progress of metal dusting has been widely described throughout the years. However, the initial stage of metal dusting has been less studied.

Metal dusting is initiated by unwanted carbon formation on the metal surface and carbon formation especially on Fe, Ni and their alloys and it is kinetically controlled. In other words, it is strongly influenced by temperature, partial pressure of gases, alloy composition and nanostructure of alloy. For example, carbon formation tendency is different when the composition of a synthesis gas is changing, since the tendency of carbon formation is a function of partial pressure and temperature. Under the synthesis gas atmosphere, CO reduction, Boudouard reaction and alkane cracking reactions are participating in carbon formation. In case of alloy composition, Cr and Al, often included into Fe- or Ni-base alloys to produce a protecting oxide layer on the metal surface against carburization reactions. When it comes to nanostructure of alloy, grain size and surface finishing are the factors affecting carbon formation. These will be further discussed in **Chapter 2**.

The goal of this paper is to study the temperature effects on the initial stage of metal dusting corrosion. The effects of pre-treatment and CO exposure temperature on surface carbon formation will be explained by experimental investigation. The effect of the different time scale of CO exposure is also studied. After the experiments, the surface of samples will be further characterized by optical microscopy and scanning electron microscopy (SEM).

2. Theory and Literature review

2.1 Thermodynamics

Metal dusting is the result of unwanted carbon formation on the inner surface of equipment under a synthesis gaseous atmosphere at high temperature (400-800 °C) with low oxygen/ steam partial pressure. It can be found in synthesis gas production plant, especially inner surface of reformer equipment. Synthesis gas consists with CO, CO_2, H_2, H_2O and trace of CH_4. Under this gaseous atmosphere at high temperature, unwanted carbon is produced by CO reduction reaction (water-gas reaction) and Boudouard reaction. Tendency of carbon formation can be presented by a thermodynamic parameter, carbon activity (a_c). It is a function of temperature and partial pressure of gas components. A number of researches have reported that metal dusting starts when the gas phase carbon activity is greater than unity ($a_c \gg 1$) [1, 3, 10].

- CO reduction reaction (Water-gas reaction)

$$CO_{(g)} + H_{2\,(g)} \leftrightarrow C_{(s)} + H_2O_{(g)} \qquad \Delta H^{\circ}_{298} = -131.3 \text{ kJ/mol} \qquad \textbf{(2.1)}$$

$$a_{C_1} = K_1(T)\left[\frac{P_{CO}P_{H_2}}{P_{H_2O}}\right] \qquad\qquad \textbf{(2.2)}$$

where K_i = equilibrium constant of the reaction

P_i = partial pressure of gas component i

- Boudouard reaction

$$2CO_{(g)} \leftrightarrow C_{(s)} + CO_{2(g)} \qquad\qquad \Delta H^\circ_{298} = -172.4 \text{ kJ/mol} \qquad\qquad \textbf{(2.3)}$$

$$a_{C_2} = K_2(T)\left[\frac{P_{CO}{}^2}{P_{CO_2}}\right] \qquad\qquad\qquad\qquad \textbf{(2.4)}$$

Since the synthesis gas includes CO, CO_2, H_2 and H_2O, water-gas shift reaction can also occur. Water-gas shift reaction does not make any carbon on the surface, but it changes gas composition.

- Water-gas shift reaction

$$CO_{(g)} + H_2O_{(g)} \leftrightarrow CO_{2(g)} + H_{2(g)} \qquad\qquad \Delta H^\circ_{298} = -41.2 \text{ kJ/mol} \qquad\qquad \textbf{(2.5)}$$

Sometimes hydrocarbons are present in the gas mixture. Then, alkane cracking reactions may happen.

- Alkane cracking

$$C_nH_{2n+2\,(g)} \leftrightarrow nC_{(s)} + (n+1)H_{2\,(g)} \qquad\qquad \Delta H > 0 \qquad\qquad \textbf{(2.6)}$$
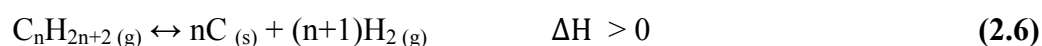
Where n=1, methane decomposition reaction can be obtained.

- CH_4 decomposition

$$CH_{4\,(g)} \leftrightarrow C_{(s)} + 2H_{2\,(g)} \qquad\qquad \Delta H^\circ_{298} = 75.6 \text{ kJ/mol} \qquad\qquad \textbf{(2.7)}$$

$$a_{C_3} = K_3(T)\left[\frac{P_{CH_4}}{P_{H_2}{}^2}\right] \qquad\qquad\qquad\qquad \textbf{(2.8)}$$

CO reduction (**2.1**) and Boudouard (**2.3**) reactions are exothermic. Thus, low temperature (T < 400 °C) is favored by thermodynamics. At the high temperature (T > 800 °C), however, reaction kinetics are faster. Hence, temperature for reaction (**2.1**) and (**2.3**) is optimum in between 400-800 °C.

On the other hand, CH_4 decomposition reaction (**2.7**) is endothermic which means high temperature is favored by thermodynamics. Reaction kinetics is slow when the temperature is less than 1000 °C [11].

There are other reactions which may form carbon during the metal dusting.

$$CO_{(g)} + Me_{(s)} \leftrightarrow C_{(s)} + MeO_{(s)} \qquad\qquad (2.9)$$

$$CO_{2\,(g)} + 2Me_{(s)} \leftrightarrow C_{(s)} + 2MeO_{(s)} \qquad\qquad (2.10)$$

where   Me = metal particle, especially Fe and Ni

         MeO = metal oxide

2.2 Kinetics

As already mentioned in **Chapter 1**, surface carbon formation is kinetically controlled. Kinetics is influenced by the local conditions like temperature and partial pressure. Local conditions, concentration (partial pressure) and temperature, at the surface of alloy might be different from the overall conditions because of the mass and heat transfer limitations. Kinetics is also influenced by the catalytic properties such as composition and nanostructure of alloy.

2.2.1 Effects of different elements in alloys

The metal dusting corrosion phenomenon is governed by oxidation and carburization. An oxide layer is important because of its function that suppresses carburization and later metal dusting. If the oxide layer is too thick, the metal alloys will have problems with thermal expansion and heat transfer. If it is too thin, however, the metal alloys cannot be protected from the corrosion. Therefore, the thickness of the oxide layer should be moderate. High Cr content increases the thickness of oxide layers. Carbon diffusion in oxides is less than in pure metals, and hence suppresses metal dusting.

On the other hand, an increase of Ni-content in Fe-base alloys decreases the carbon solubility. It will result in a decrease of carburization rate and forming less carbon [12]. Si and Al have positive effect to prevent metal dusting corrosion by forming a protective oxide layer (SiO_2 and Al_2O_3). Also, they help Cr to develop a protective oxide layer by increasing Cr diffusivity from the bulk to the alloy surface [6]. Meanwhile, sulfur is strongly adsorbed on the surface of alloys and disturbs the surface reactions [6].

2.2.2 Effects nanostructure of alloy

In the temperature window (400-800 °C) where metal dusting is dominant, Cr-oxide formation is not guaranteed. It depends on the microstructure of the alloy material; *i.e.* grain size and surface deformation (grinding and polishing) [13].

- Grain size

Oxide formation is favored by a fine grained microstructure [14]. A research from Grabke, H. *et al.* demonstrates that smaller grain size transfer Cr rapidly from the bulk to the surface along by short diffusion paths.

- Surface deformation

Dislocations and grain boundaries from surface deformation act as fast diffusion paths which supply Cr to the surface and form a protective oxide layer [6]. According to Grabke *et al.*, there are more grain boundaries and dislocations in the ground specimens than in as-receive or electro-polished surfaces [6]. To prove this statement, Grabke carried out a laboratory exposure experiment. Three different types of surface deformations were exposed in $CO(2\%)$-$H_2(24\%)$-H_2O mixture at 650 °C for 3000 h: (1) as-receive (black); (2) electro-polishing; (3) grinding. From the result (**Figure 2.1**), it is turned out that ground materials perform better than the others [6].
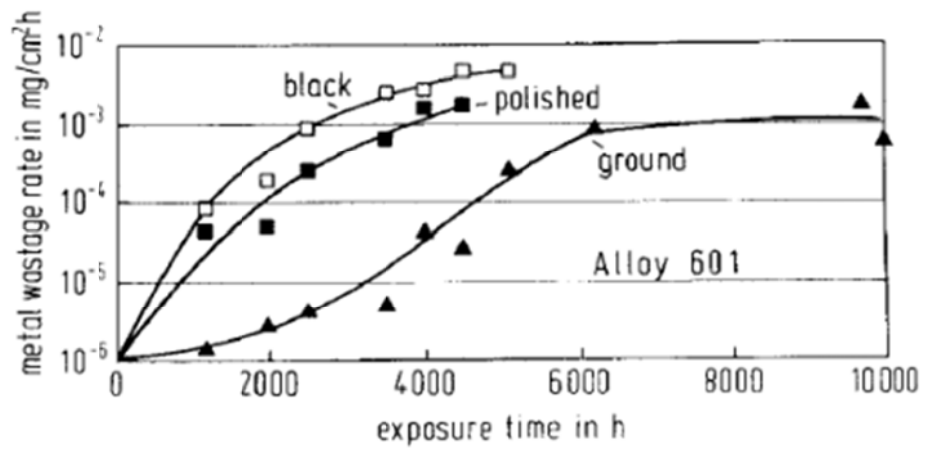
Figure 2.1 Exposures of Ni-base alloys in CO(2%)-H$_2$(24%)-H$_2$O mixture at 650 °C for Alloy 601 in three different surface states: black (as-receive); polished; ground [6].

2.3 Mechanism

Several mechanisms of the metal dusting on Fe, Ni and their alloys were suggested. The most widely accepted mechanism was proposed by Grabke *et al.* [15]. A schematic explanation is given in **Figure 2.2**.

(i)   Carbon is transferred from gas phase ($a_c > 1$) to solid surface of material.

$$CO + H_2 \rightarrow C_{(dissolved)} + H_2O \tag{2.11}$$

(ii)   Forming carbide on the material surface when the material is supersaturated with solid solution of carbon.

$$3Fe_{(s)} + C_{(dissolved)} \rightarrow Fe_3C_{(s)} \tag{2.12}$$

(iii)   Graphite nucleates on the carbide surface and a_c decreases at graphite-carbide interface because carbon transfer is retarded by carbide and carbon accumulate on the surface.

$$CO + H_2 \rightarrow C_{(graphite)} + H_2O \tag{2.13}$$

(iv)   Carbide at interface of graphite-carbide decomposes into fine metal particles and graphite under low a_c ($a_{c,Interface} < a_{c,Fe_3C}$).

$$Fe_3C_{(s)} \rightarrow 3Fe_{(s)} + C_{(graphite)} \tag{2.14}$$

(v)   Fine metal particles diffuse to gas phase and catalyze the formation of solid carbon.
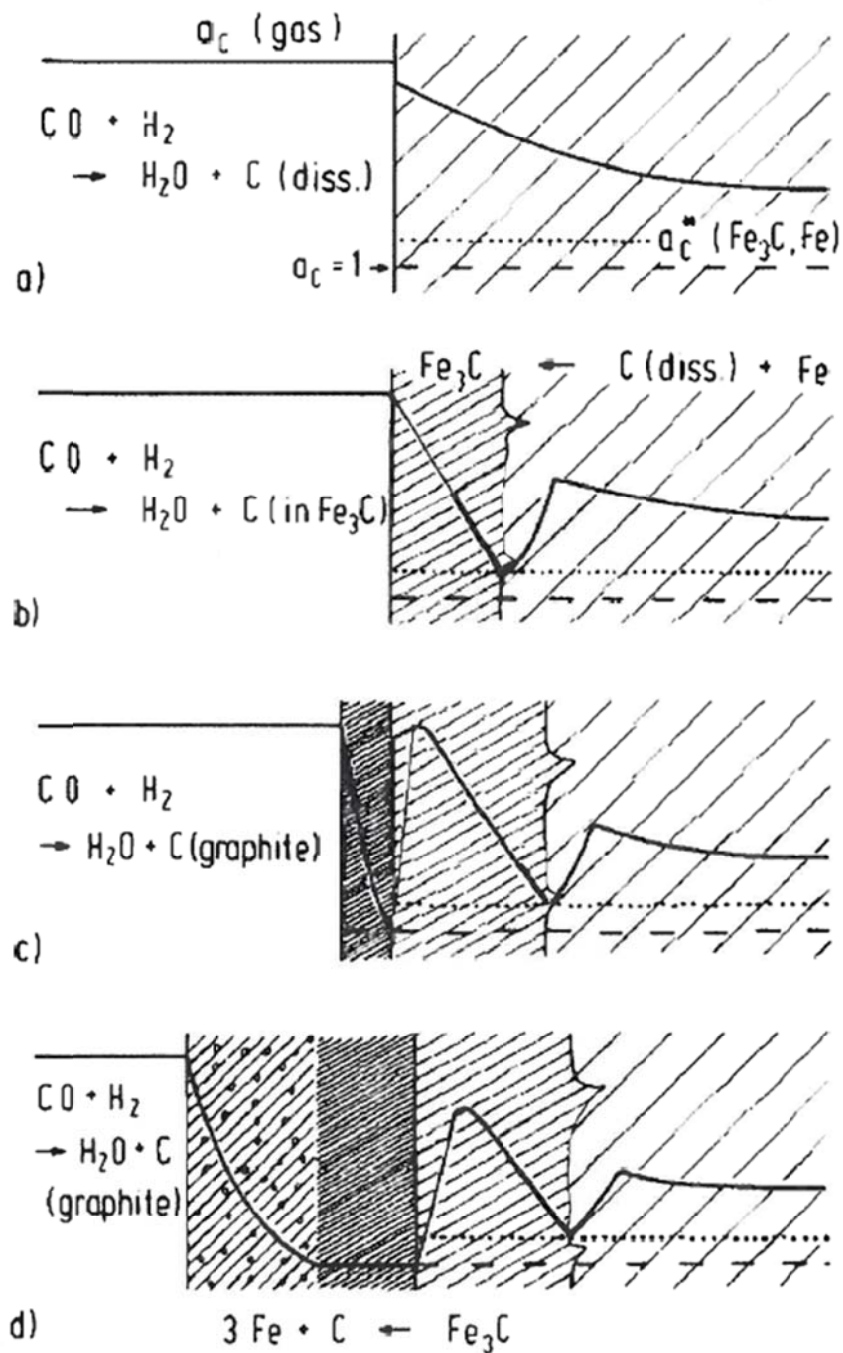
Figure 2.2 Schematic illustration of metal dusting mechanism: a) Carbon is transferred from gas phase (a_c>1) to solid surface of Fe; b) Forming carbide on the Fe surface when the material is supersaturated with solid solution of carbon; c) Graphite is deposited on the carbide surface; d) Carbide decomposes into fine metal particles and graphite [15].

Possible steps for the carbon transfer from the gas phase to solid surface of material **(2.11)** are reported in literatures and it is listed in **Table 2.1**. * indicates vacant site and *A** represents adsorbed species on the surface. Underlined reactions are the rate determining steps (RDS).

Table 2.1 Mechanistic steps for carbon formation via CO reduction, Boudouard and CH$_4$ decomposition reactions [1].

CO reduction reaction	Boudouard reaction	CH$_4$ decomposition reaction
$CO_{(g)} + * \leftrightarrow CO*$	$CO_{(g)} + * \leftrightarrow CO*$	$CH_{4(g)} + * \leftrightarrow CH_4*$
$\underline{\mathbf{CO* + * \leftrightarrow C* + O*}}$	$CO* + * \leftrightarrow C* + O*$	$CH_4* + * \leftrightarrow CH_3* + H*$
$H_{2(g)} + 2* \leftrightarrow 2H*$	$\underline{\mathbf{CO* + O* \leftrightarrow CO_2* + *}}$	$\underline{\mathbf{CH_3* + * \leftrightarrow CH_2* + H*}}$
$H_{2(g)} + O* \leftrightarrow H_2O_{(g)} + *$	$\underline{\mathbf{CO_2* \leftrightarrow CO_{2(g)} + *}}$	$CH_2* + * \leftrightarrow CH* + H*$
$H_2O_{(g)} + * \leftrightarrow H_2O*$	$\underline{\mathbf{CO_{(g)} + O* \leftrightarrow CO_{2(g)} + *}}$	$CH* + * \leftrightarrow C* + H*$
$H_2O* + * \leftrightarrow OH* + H*$	$nC* \leftrightarrow nC_{(s)} + n*$	$nC* \leftrightarrow nC_{(s)} + n*$
$OH* + * \leftrightarrow O* + H*$	$C* \leftrightarrow C_{(dissolved)} + *$	$C* \leftrightarrow C_{(dissolved)} + *$
$2OH* \leftrightarrow H_2O* + O*$		
$nC* \leftrightarrow nC_{(s)} + n*$		
$C* \leftrightarrow C_{(dissolved)} + *$		

2.4 Metal dusting corrosion of different materials

The mechanism for Fe-base alloy and Ni-base alloys was explained in **Chapter 2.3**. It is widely accepted, however, degradation mechanisms change when composition of alloys changes.

2.4.1 Metal dusting of Ni-base alloys

As already illustrated in **Figure 2.2**, Fe-base alloys and Ni-base alloys form a carbide, $(Fe, Ni)_3C$, as an intermediate. However, Grabke suggested that Ni-base materials with more than 40% of Ni decompose directly, not via a carbide [6, 16]. Metal dusting mechanism of Ni-base alloys is shown in **Figure 2.3**.

Metal particles escaped from metal dusting of Ni and Ni-base alloys are relatively larger than the particles released from metal dusting of Fe and low-alloy steels[10]. Bigger particles have lower catalytic activity for graphite deposition and this result in slower metal dusting rate. Thus, the metal dusting rate are declining with increasing Ni content of alloy [1].

2.4.2 Metal dusting of Fe and low-alloy steels

Low-alloy steels which contain low contents of Cr are attacked by general metal wastage unlike high-alloy steels having pitting and formation of holes [1, 5]. **Figure 2.3** shows degradation mechanism of Fe, low-alloy steels and Ni.
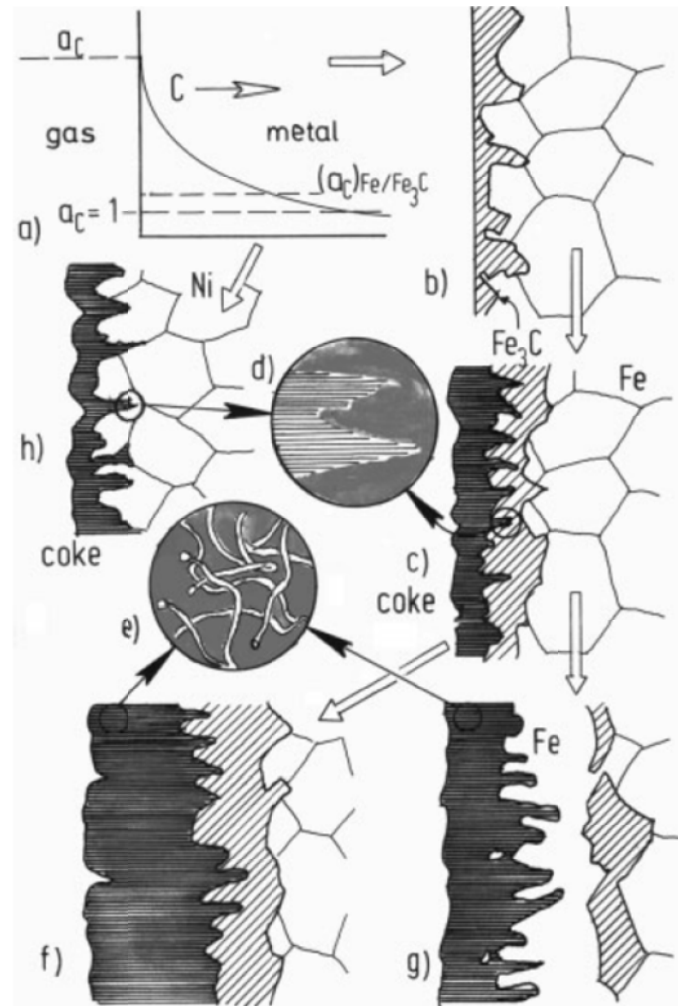
Figure 2.3 Schematic explanation of processes in metal dusting of Fe, low-alloy steels, Ni and Ni-alloys: a) Carbon is transferred from gas phase (a_c>1) to solid surface of low-alloy steels; b) Cementite (Fe$_3$C) layer is formed on the surface of Fe and low-alloy steels; c) Graphite grows into the carbide (cementite) layer; d) Graphite lattice planes grow perpendicular to carbide layer; e) Carbon filament grows behind the particles detached from carbide decomposition; f) Steady state of metal dusting when temperature is lower than 600 °C, Fe$_3$C grows inward; g) Steady state of metal dusting when temperature is higher than 700 °C, formation of Fe layer which cause disappearance of Fe$_3$C layer by diffusing carbon; h) Inward graphite grows on the surface of Ni and Ni-base alloys without formation of carbide layer [6].

2.4.3 Metal dusting of high-alloy steels

High-alloy steels which have high Cr content [1] produce a protective Cr-oxide layer. However, a metal dusting phenomenon may begin because of defects in the oxide layer. Metal dusting of high-alloy steels causes pitting and formation of holes [5]. **Figure 2.4** illustrates the proposed steps of metal dusting of high-alloy steels [6].
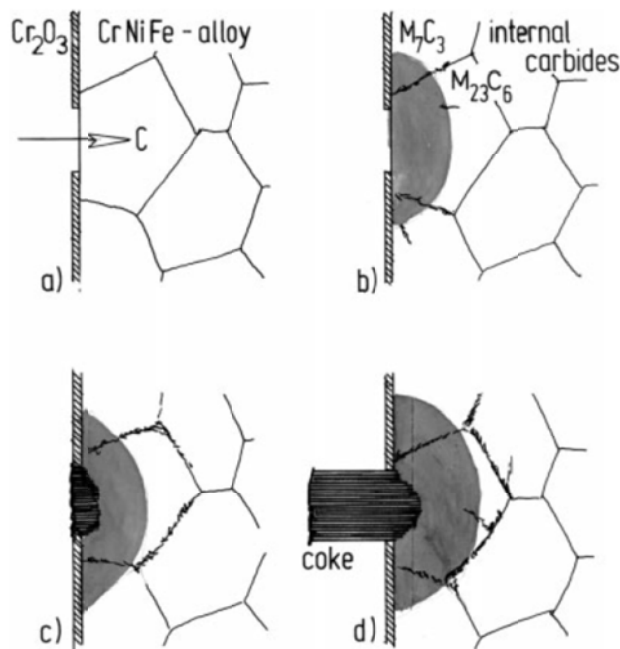
Figure 2.4 Schematic description of processes in metal dusting of high-alloy steels: a) Carbon is transferred from gas phase to solid surface of high-alloy steels through a defect in the oxide layer; b) Internal carbides are formed from dissolved carbon; c) Inward graphite grows after dissolved carbon oversaturation; d) Coke grows outward which include graphite, metal, carbide *etc* [6].

3. Material and Methods

3.1 Material

Inconel 601 is an industrial alloy mostly consisted of nickel, chromium and iron. It has outstanding resistance to oxidation and high-temperature corrosion. As well as resistance to oxidation and corrosion, it also has good mechanical properties. **Table 3.1** shows properties of Inconel 601.

Table 3.1 Properties of Inconel 601 [17].

LIMITING CHEMICAL COMPOSITION (%)	Ni......58.0 – 63.0 Cr......21.0 – 25.0 Al ....1.0 – 1.7	Fe......Remainder C..........0.10 max. Mn......... 1.0 max.	Si.........0.50 max. S....... 0.015 max. Cu......... 1.0 max.
PHYSICAL CONSTANTS AND THERMAL PROPERTIES	Density Melting Range Specific Heat Coefficient of Expansion Thermal Conductivity Electrical Resistivity	g/cm^3 °C J/kg•°C 20–100 °C, μm/m •°C W/m •°C μΩ•m	8.11 1360-1411 448 13.75 11.2 1.19

The bulk composition of Inconel 601 alloy is confirmed by Gunawardana via EPMA/WDS. The result agrees with the specifications of Inconel 601 (**Table 3.2**). The alloy is a Ni-base material (61 wt. %) with Cr (23 wt. %) and Fe (13 wt. %). 1 wt. % of Al, 0.6 wt. % of Mn and Ti, Si and C also exist.

Table 3.2 Bulk composition of Inconel 601 alloy, determined by EPMA/WDS [1].

Composition basis	Element percentage (%)								
	Ni	Cr	Fe	Al	Mn	Ti	Si	Cu	C
Avg. atomic	57.65	24.31	13.33	2.64	0.60	0.36	0.15	0.17	0.77
Avg. weight	60.82	22.71	13.38	1.28	0.60	0.31	0.08	0.19	0.17

3.2 Sample preparation

First, Inconel 601 sheet (0.5mm thickness) was cut into $15 \times 8mm^2$ size samples. Cut samples one by one stick to a plastic cube by using double side tape and then proceed the grinding step to remove surface defect and/or unevenness. After the grinding step, the surface of the alloy will be flat and have a more controlled composition. The samples were ground with P320 (45 µm), P800 (20 µm) and P2000 (10 µm) grit SiC papers.

After removing the damage by grinding, a polishing process has been conducted. Polishing consists of steps of continuous abrasion by fine particles. As an abrasive material, diamond dust is used, which works very effectively because of its hardness. The samples were polished with 6 µm, 3 µm and 1 µm sized diamond dust.

Thereafter the samples were cleaned with ethanol and water and investigated by optical microscope. In the case of serious scratches, the grinding and polishing steps should be repeated.

Finally, the samples were cleaned ultrasonically in hexane (99%) and dried overnight.

3.3 Setup settings

Before the experiments started, risks were evaluated. By assessing the risks, possible hazard can be prevented. Risk evaluation data are attached as an appendix (**Appendix. A**). The main risk of this experiment is using CO gas. CO gas is poisonous and it causes headache, dizziness and nausea when people inhale this gas. In severe cases, they may even die. To handle this problem, a CO gas detector was used and leak tests were performed before every experiment. During the experiments, the gas alarm was turned on.

After the risk assessment, a calibration of flowmeters was performed. The calibration is a comparison between the quantity obtained by measuring instrument and the set values. By doing a calibration, the accuracy of the reading can be increased. Gas flowmeters can be calibrated using mass or volume of the gas. A soap-film burette, bubble flowmeter (**Figure 3.1**), is used to calibrate the flow controllers in the setup. Calibration data for the flow controllers are given in **Appendix. B**.

Figure 3.1 A soap-film burette [18].

Figure 3.2 shows a simplified flow diagram of the reactor setup used for experiments. A detailed setup is shown in **Appendix. C**. The inside of the reactor was plated with gold to minimize the metal dusting phenomenon on the surface of the reactor (**Figure 3.3**) [1]. Alloy samples were tested one at a time and hung inside the reactor using a three segments quartz rod. All the exposure experiments were carried out at 1 bar.

Once the sample was loaded, leak tests were performed overnight with Argon. Then, the reactor was flushed with Ar gas for 20 minutes at room temperature.
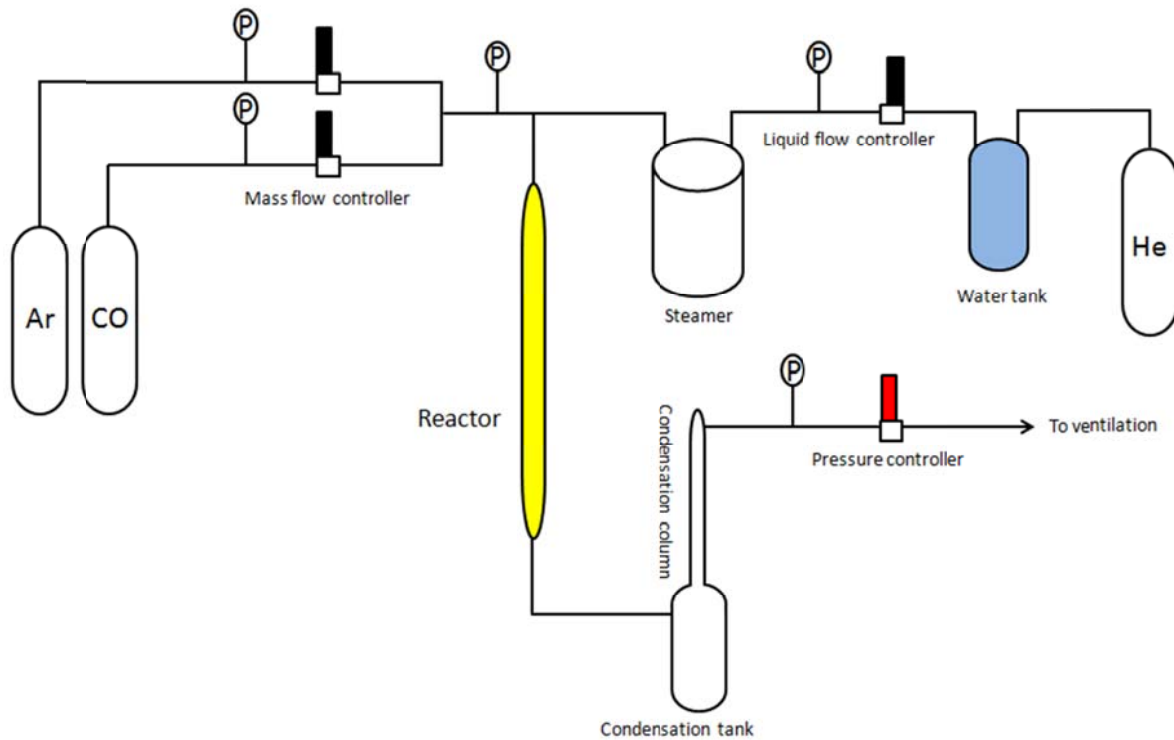
Figure 3.2 Schematic diagram of setup.
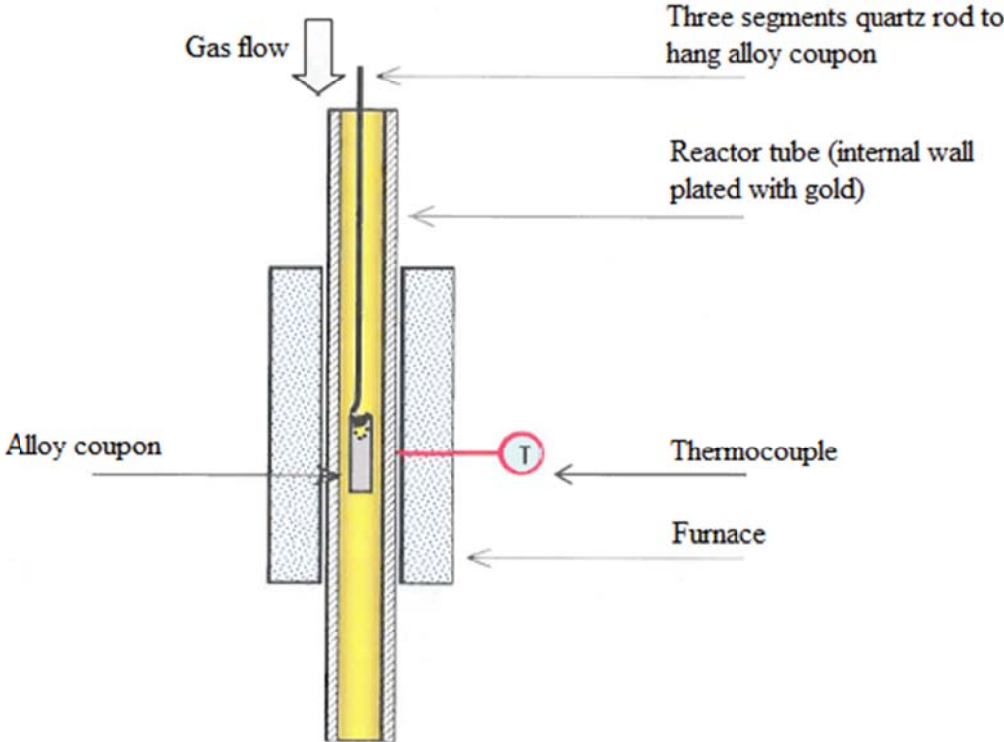
Figure 3.3 Schematic of inside the reactor [1].

3.4 Sample exposures

3.4.1 Oxidation treatments

Oxidation treatments were conducted while keeping pressure at 1 bar and increasing the temperature from room condition to the desired temperature (540 °C or 760 °C). These temperatures are selected to cover the temperature window of 'low-medium-high'. 540 °C is considered as low temperature oxidation, and 980 °C is taken as high temperature oxidation. For safety reasons, however, high temperature oxidation treatments have not been performed. Total gas flow rate was 100 Nml/min, and the composition of the gas mixture was 10% steam in Ar. The ramping rate was 10 °C/min. Once it reached the desired temperature, the sample was dwelled for 6 h. After 6 h, CO exposure treatment was carried out immediately.

3.4.2 CO exposure treatments

After the oxidation treatments, the sample was ramped up/down to a certain temperature (650 °C or 750 °C) at 1 bar. Total gas flow rate was at 100 Nml/min with 100% Ar and the ramping rate was 10 °C/min. When it reached desired temperature, the sample was dwelled for 20 minutes or longer to stabilize the temperature in the system. CO exposure treatment is very sensitive to temperature, so keeping exact temperature is important. Once the measured temperature equaled to the set value, CO was induced with 10 Nml/min. Total flow rate is 100 Nml/min and the composition is 10% CO and 90% Ar. CO exposure treatment was carried out with different dwelling time; 1 h, 2 h, 5 h and 20 h. **Figure 3.4** shows the temperature control profile of exposure treatments and the test matrix is in **Table 3.3**. All the results (figures) will be shown and explained in **Chapter 4**.

(a)
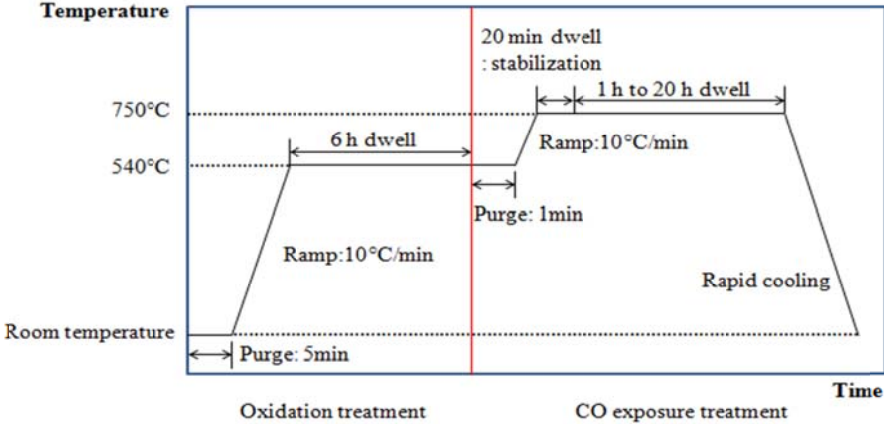
(b)
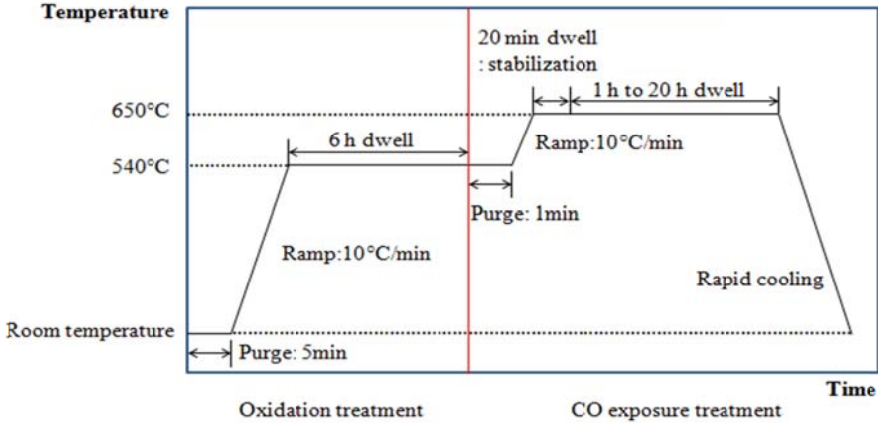
(c)
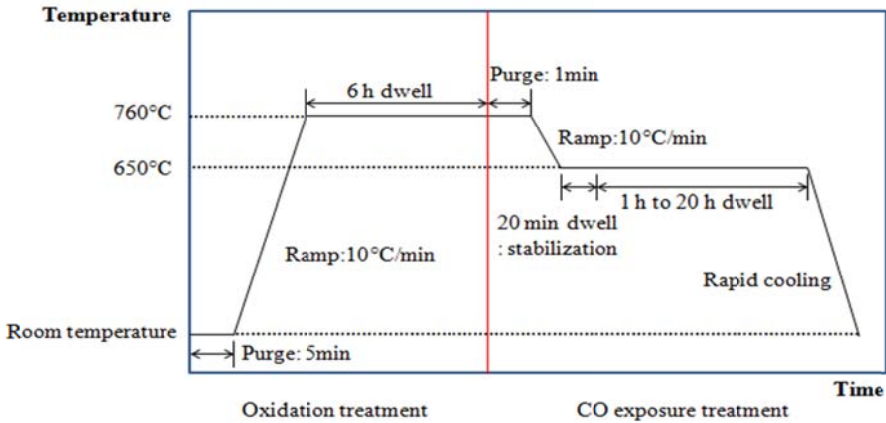
Figure 3.4 Temperature profile: (a) Oxidation treatment at 540 °C and CO exposure treatment at 750 °C; (b) Oxidation treatment at 540 °C and CO exposure treatment at 650 °C; (c) Oxidation treatment at 760 °C and CO exposure treatment at 650 °C.

24

Table 3.3 Test matrix

Case	Oxidation exposure temperature	CO exposure temperature	Oxidation exposure time	CO exposure time	Result
1 - 1				1 h	**Figure 4.1 (a), Figure 4.2 (a)**
1 - 2	540 °C	760 °C	6 h	2 h	**Figure 4.1 (b), Figure 4.2 (b)**
1 - 3				5 h	**Figure 4.1 (c), Figure 4.2 (c)**
1 - 4				20 h	**Figure 4.1 (d), Figure 4.2 (d)**
2 - 1				1 h	**Figure 4.4 (a), Figure 4.5 (a)**
2 - 2	540 °C	650 °C	6 h	2 h	**Figure 4.4 (b), Figure 4.5 (b)**
2 - 3				5 h	**Figure 4.4 (c), Figure 4.5 (c)**
2 - 4				20 h	**Figure 4.4 (d), Figure 4.5 (d)**
3 - 1				1 h	**Figure 4.6 (a), Figure 4.7 (a)**
3 - 2	760 °C	650 °C	6 h	2 h	**Figure 4.6 (b), Figure 4.7 (b)**
3 - 3				5 h	**Figure 4.6 (c), Figure 4.7 (c)**
3 - 4				20 h	**Figure 4.6 (d), Figure 4.7 (d)**

3.5 Characterization techniques

3.5.1 Optical microscopy

The samples were characterized with optical microscopy and scanning electron microscopy (SEM). Overall tendency of carbon formation on the alloy surface can be observed through optical microscope, Leica DC 300.

3.5.2 Scanning electron microscopy (SEM)

Samples after CO exposure were investigated by using Hitachi SU-6600, field emission scanning electron microscope. Topographical information on the surface can be obtained as a visual image by the SEM. In SEM, a finely focused electron beam is used for the imaging while the optical microscope is using light. **Figure 3.5** illustrates the differences between an optical microscope (light microscope) and a scanning electron microscope.

Figure 3.6 shows a schematic diagram of the SEM. The electron beam is generated from the filament by two types of beam emission: Thermal emission and Field emission [19]. Thermal emission uses heat to release the electrons from the filament. Filaments for thermal emission (Tungsten, LaB_6) are relatively cheap, however, they last short. In field emission, the electrons are excited magnetically. The filament acts as a cathode, which is negatively charged, while the anode is positively charged. The potential difference between the cathode and the anode releases the electrons off. This type of emission is cool, so filament lasts longer.
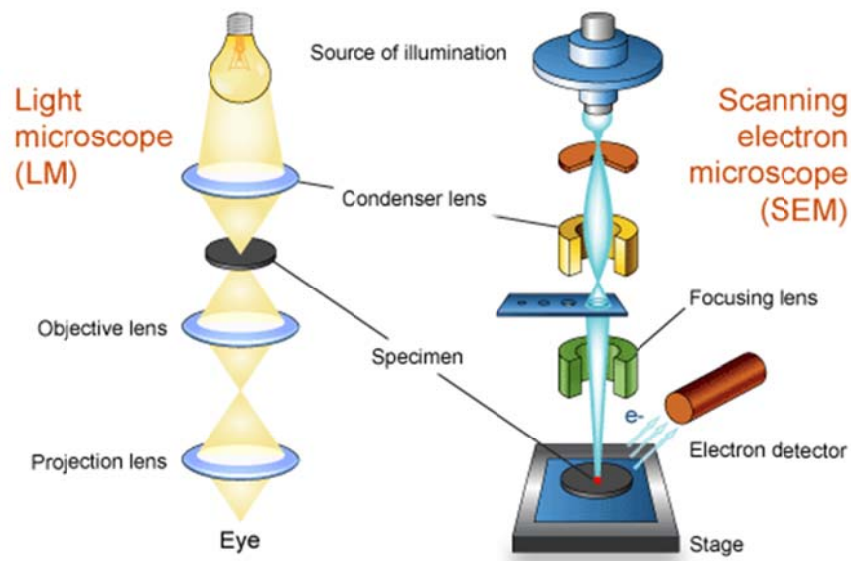
Figure 3.5 Comparison of optical microscope (light microscope) and scanning electron microscope [20].
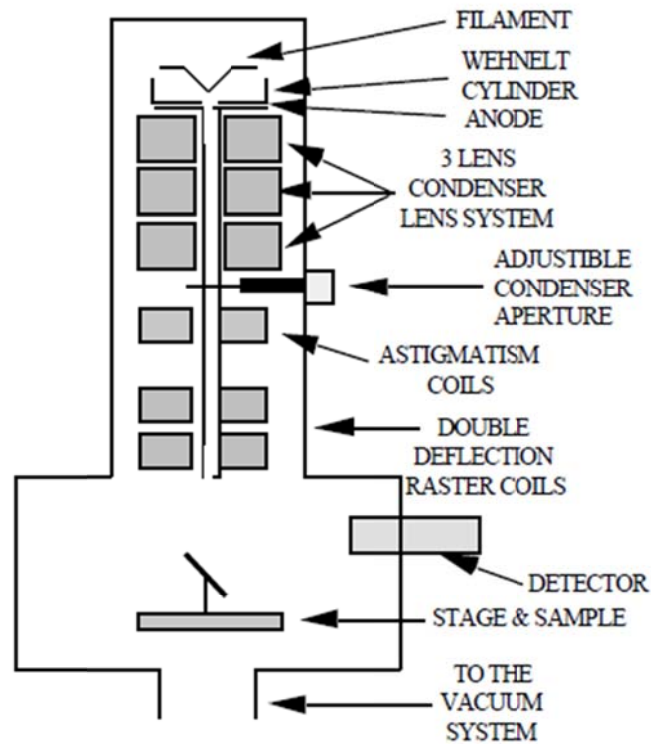
Figure 3.6 Schematic diagram of scanning electron microscope [19].
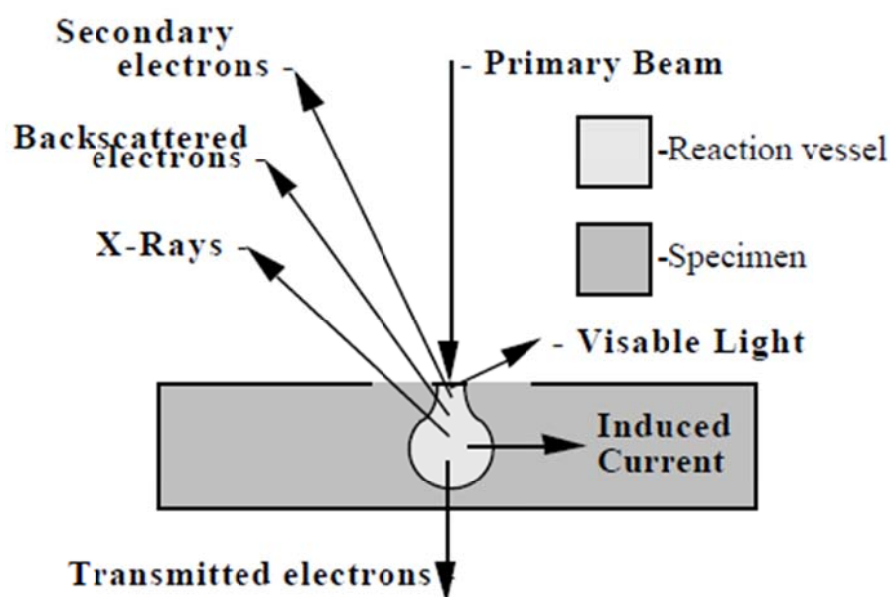
Figure 3.7 Different types of interactions between electron beam and the specimen [19].

The electron beam generates several signals when it interacts with the specimen. Each of signals has different energy, so it can be detected by different detectors. **Figure 3.7** shows different types of interactions between the electron beam and the specimen. Secondary electrons (SE) are the most commonly used because of excellent features about imaging which are high depth of focus and high resolution. High depth of focus means SEM can focus on different heights at the same time. Depth of focus and resolution are influenced by the beam spot size, working distance, aperture size, *etc*. Electron beam shape, size, and the position on the surface of specimen are controlled by lenses and coils [19]. For all the SEM images, which will be shown in **Chapter 4**, SE mode was used.

SEM is basically used to study the surface topography or morphology of a given surface. In addition to that composition analysis, crystallographic features and electronic properties can also be obtained by various different detectors mounted with the microscope.

4. Results and Discussion

All micrographs that are shown in this chapter represents the surface of Inconel 601 samples which are pre-oxidized with 10% steam-Ar gas at 1 bar for 6 h at different temperatures. Right after the oxidation treatments, samples are exposed to 10% CO-Ar gas at 1 bar at different temperature for different time scale. All samples are ground and polished before the oxidation treatments as described in **Chapter 3.2**.

4.1 Effect of CO exposure time

(a)　　　　　　　(b)　　　　　　　(c)　　　　　　　(d)

Figure 4.1 Optical micrographs of pre-oxidized (10% steam-Ar gas, 540 °C, 1 bar, 6 h) and CO exposed (10% CO-Ar gas, 750 °C, 1 bar) Inconel 601 samples. CO exposed for: (a) 1 h; (b) 2 h; (c) 5 h; (d) 20 h.

Figure 4.1 (a-d) shows optical micrographs of polished Inconel 601 samples pre-oxidized at 540 °C, and then exposed to CO/Ar mixture at 750 °C for 1 h, 2 h, 5 h and 20 h respectively. All samples seem to have carbon on the surface due to their black surface. To check for

surface carbon formation samples were further characterized by SEM. In the case of the second specimen (**Figure 4.1 (b)**), the brighter part, *i.e.* dominant area, was studied by SEM.

(a)

(b)

(c)

(d)

Figure 4.2 SEM micrographs of pre-oxidized (10% steam-Ar gas, 540 °C, 1 bar, 6 h) and CO exposed (10% CO-Ar gas, 750 °C, 1 bar) Inconel 601 samples. CO exposed for: (a) 1 h; (b) 2 h; (c) 5 h; (d) 20 h.

Figure 4.2 (a-d) compares SEM micrographs of pre-oxidized Inconel 601 samples after CO exposure at 750 °C. Straight lines on the surface observed in **Figure 4.2 (c)** are results of the grinding and polishing steps. Crystal-like features are present on the surface of all samples in **Figure 4.2 (a-d)**. Similar observations were reported by Gunawardana *et al.* [1] in his study of oxidation of Inconel samples at various high temperature condition treatments. As they reported, those particles are oxides of Cr with small amount of Ni, Fe and other elements (Al, Si, Ti, *etc.*) [1]. SEM micrographs indicate that there are no carbon on the samples which are exposed to CO/Ar gas mixture less than 2 h (**Figure 4.2 (a-b)**). Filaments carbon on the sample exposed to CO for 5 h were not easily detected by low magnification imaging as shown by (**Figure 4.2 (c)**). But at high magnification carbon filaments were observed and shown in the **Figure 4.3**. Arrows in the **Figure 4.2 (d)** and **Figure 4.3** point the carbon filaments.
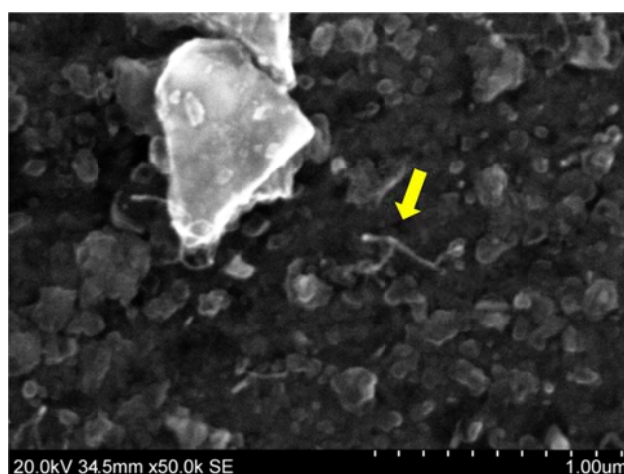
Figure 4.3 SEM micrographs of surface carbon formation of pre-oxidized (10% steam-Ar gas, 540 °C, 1 bar, 6 h) and CO exposed (10% CO-Ar gas, 750 °C, 1 bar, 5 h) Inconel 601 sample.

Optical micrographs of Inconel 601 pre-oxidized at 540 °C and exposed to CO/Ar gas mixture at 650 °C for 1 h, 2 h, 5 h and 20 h respectively are shown in **Figure 4.4**. Colors of all samples are totally black and they seem to have significant amounts of carbon on the surface.

(a) (b) (c) (d)
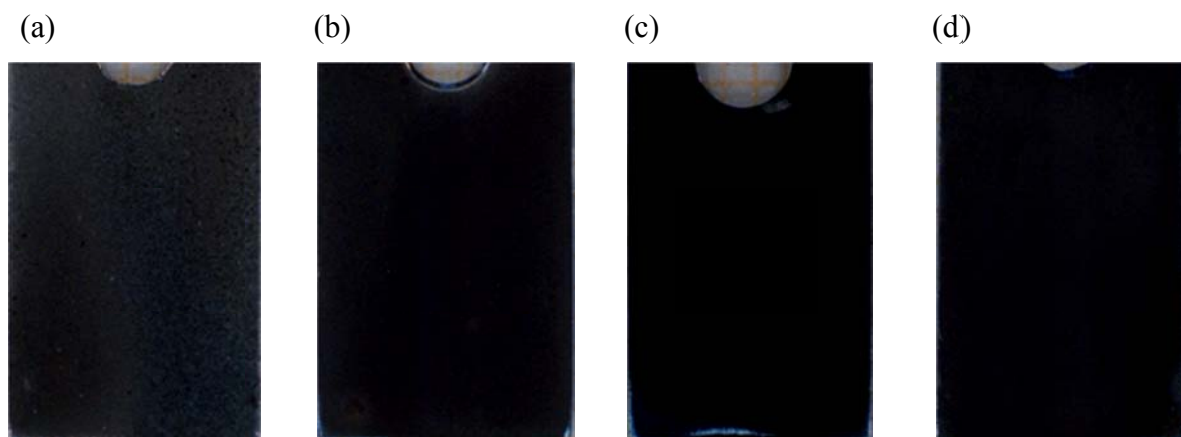
Figure 4.4 Optical micrographs of pre-oxidized (10% steam-Ar gas, 540 °C, 1 bar, 6 h) and CO exposed (10% CO-Ar gas, 650 °C, 1 bar) Inconel 601 samples. CO exposed for: (a) 1 h; (b) 2 h; (c) 5 h; (d) 20 h.

The results of SEM characterization are in **Figure 4.5**. In **Figure 4.5**, a growing trend of carbon filament can be seen. When the alloy sample is exposed to CO for 1 h, short carbon fibers exist on the surface (**Figure 4.5 (a)**). Whereas for the alloy sample which was exposed to CO for 20 h (**Figure 4.5 (d)**), much longer carbon fibers exist.

(a) (b)

(c)

(d)
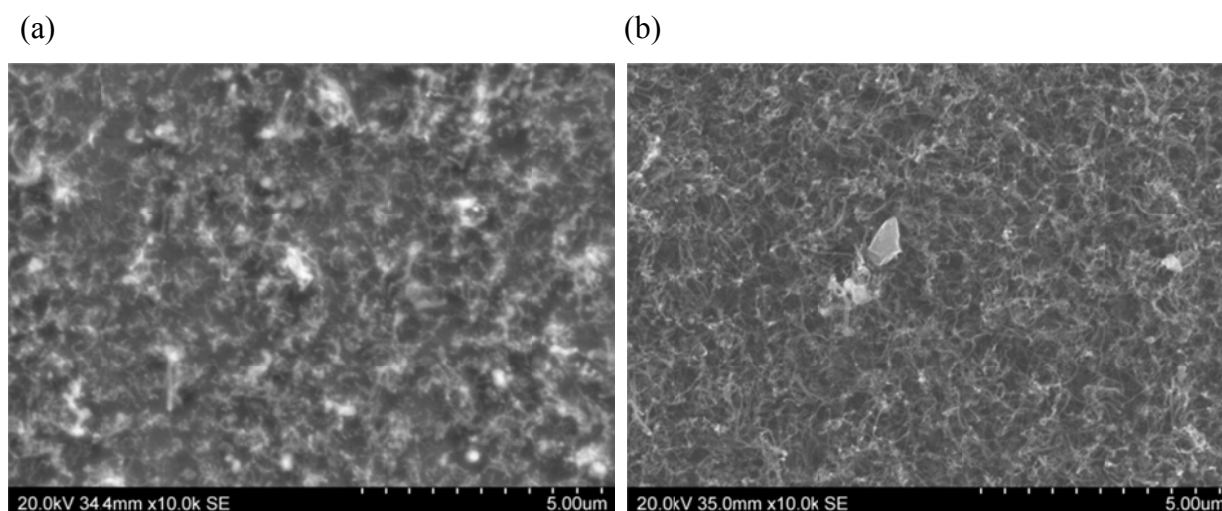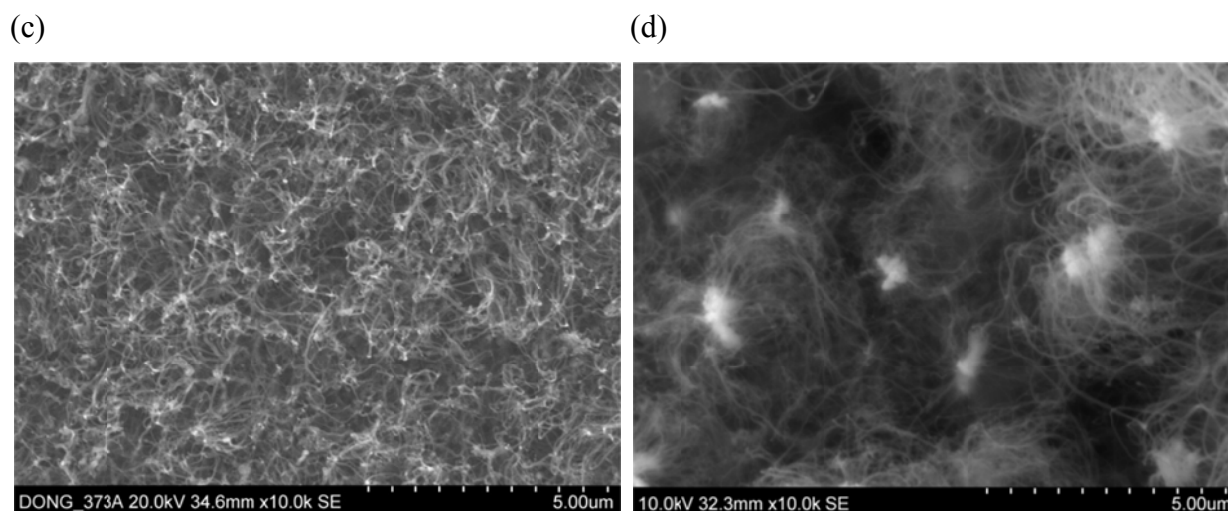
Figure 4.5 SEM micrographs of pre-oxidized (10% steam-Ar gas, 540 °C, 1 bar, 6 h) and CO exposed (10% CO-Ar gas, 650 °C, 1 bar) Inconel 601 samples. CO exposed for: (a) 1 h; (b) 2 h; (c) 5 h; (d) 20 h.

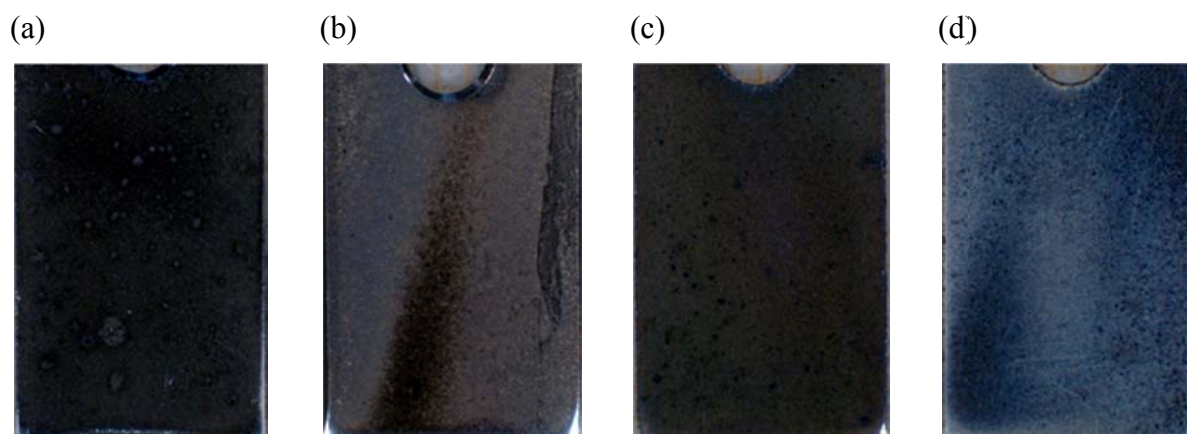(a)   (b)   (c)   (d)
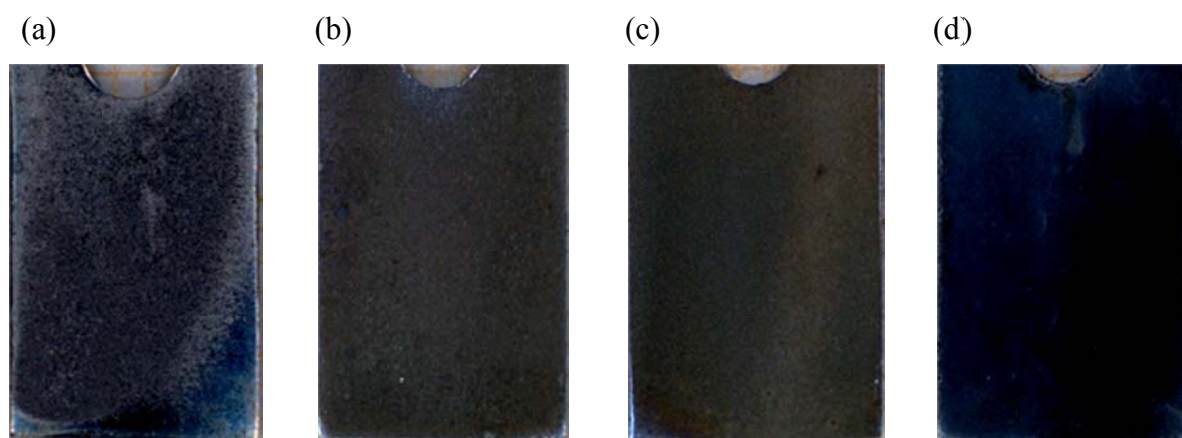
Figure 4.6 Optical micrographs of pre-oxidized (10% steam-Ar gas, 760 °C, 1 bar, 6 h) and CO exposed (10% CO-Ar gas, 650 °C, 1 bar) Inconel 601 samples. CO exposed for: (a) 1 h; (b) 2 h; (c) 5 h; (d) 20 h.

Similarly, optical micrographs of Inconel 601 pre-oxidized at 760 °C and exposed to CO/Ar gas mixture at 650 °C for 1 h, 2 h, 5 h and 20 h respectively are shown in **Figure 4.6**. Colors of all samples are black which means they seem to have carbon on the surface. In addition, an apparent tendency that specimen with longer exposure time has darker color present in **Figure 4.6**. All samples were further characterized with SEM to investigate the surface carbon formation. **Figure 4.7** is the results of SEM characterization.
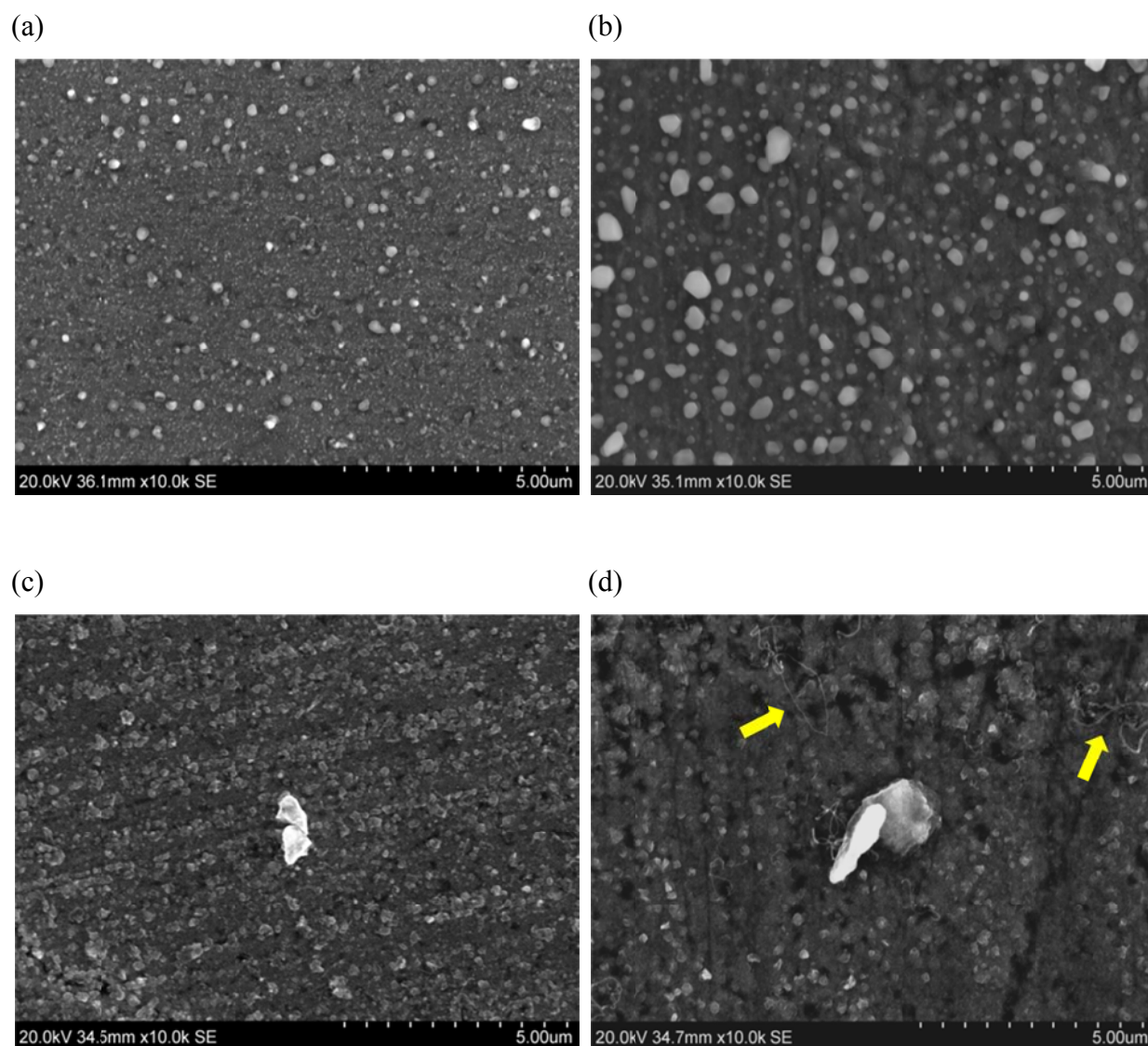
(a)

(b)

(c)

(d)

Figure 4.7 SEM micrographs of pre-oxidized (10% steam-Ar gas, 760 °C, 1 bar, 6 h) and CO exposed (10% CO-Ar gas, 650 °C, 1 bar) Inconel 601 samples. CO exposed for: (a) 1 h; (b) 2 h; (c) 5 h; (d) 20 h.

As expected, carbon filaments become longer and abundant when CO exposure treatment time is longer. The largest amount of carbon filaments were found on the fourth specimen (20 h) (**Figure 4.7 (d)**).

Some isolated unique features are identified on the sample exposed to 10% CO/Ar at 650 °C for 1 h (**Figure 4.7 (a)**). Clearer images of these growing features were taken at high magnification (**Figure 4.8 (a-b)**). To determine these features, a composition analysis could have been performed by EDS. However, EDS analysis will not be considered in this thesis.

(a)   (b)

Figure 4.8 SEM micrographs of pre-oxidized (10% steam-Ar gas, 760 °C, 1 bar, 6 h) and CO exposed (10% CO-Ar gas, 650 °C, 1 bar, 1 h) Inconel 601 sample: (a) with 20 K magnification; (b) with 50 K magnification.

The samples with very little carbon are important to study the initial stage of metal dusting because they provide an opportunity to know how the first carbon forms. By checking whether there are Ni and/or Fe particles in the oxide or not, the first step of metal dusting can be suggested. Therefore, components of the samples should be further analyzed.

The results of all these samples show that more carbon filaments are produced when they are exposed to CO gas mixture for longer time scale for the studied exposure conditions. The effect of CO exposure time has been shown in many studies and explained by kinetics of metal wastage. According to Grabke metal wastage rate could be calculated via reaction **(2.14)** [5, 15].

$$r_M = \frac{dm_M}{Adt} \left[\frac{mg}{cm^2 h} \right] \qquad (4.1)$$

where r_M = metal wastage rate

m_M = mass of alloy converted into the corrosion product

A = area

t = time

From the exposure experiments under various atmospheres, he found that the rate of metal wastage is virtually independent of time.

$$r_M = \frac{dm_M}{Adt} = k_1 \qquad (4.2)$$

$$\frac{m_M}{A} = k_1 t \qquad (4.3)$$

where k_1 = a rate constant of metal wastage

Carbon deposition determined by thermogravimetry. Fine metal particles catalyze the CO reduction reaction **(2.1)**, so it is assumed that the rate of carbon deposition is proportional to the mass of the particles [5].

$$r_C = \frac{dm_C}{Adt} = k_2 \frac{m_M}{A} \qquad\qquad (4.4)$$

$$= k_1 k_2 t \qquad\qquad (4.5)$$

where r_C = carbon deposition rate

m_C = mass of carbon deposition

k_2 = a rate constant of carbon deposition

As shown in the **Figure 4.9**, carbon deposition is proportional to the partial pressure of carbon monoxide and hydrogen and inversely proportional to the partial pressure of steam. Thus, k_2 can be expressed as below.

$$k_2 \propto \frac{p_{CO}p_{H_2}}{p_{H_2O}} \qquad\qquad (4.6)$$

$$k_2 = k \left(\frac{p_{CO}p_{H_2}}{p_{H_2O}}\right) \qquad\qquad (4.7)$$

$$r_C = \frac{dm_C}{Adt} = k_1 k\left(\frac{p_{CO}p_{H_2}}{p_{H_2O}}\right) t \qquad\qquad (4.8)$$

$$\frac{m_C}{A} = k_3 \frac{p_{CO}p_{H_2}}{p_{H_2O}} t^2 \qquad\qquad (4.9)$$

where $k_3 = k_1 k$ = a rate coefficient

From the equation **(4.3)** and **(4.9)**, it is clear that the amount of carbon deposition on the surface is increasing when CO exposure time increases.

(a)

(b)

(c)
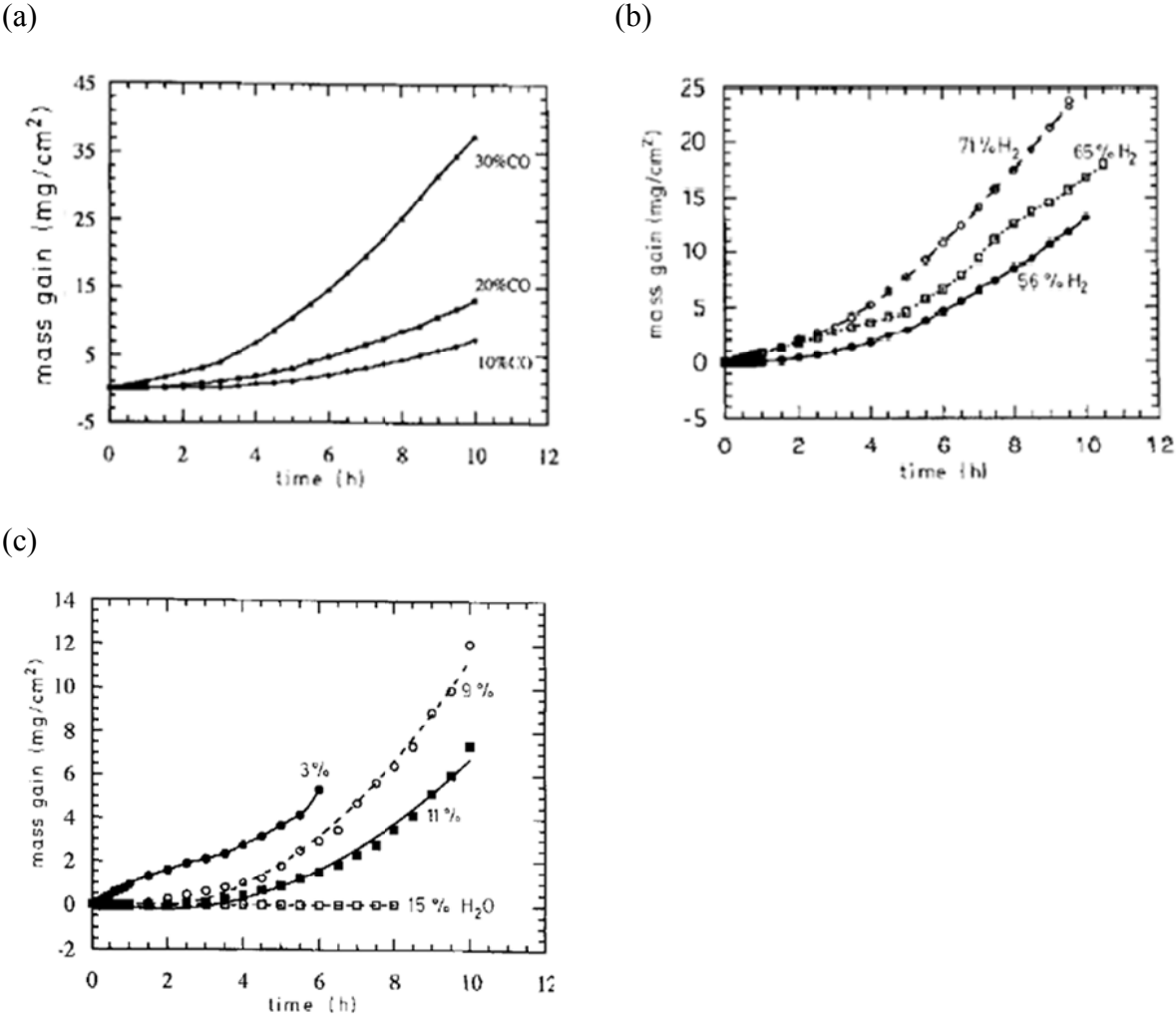
Figure 4.9 Carbon deposition experiments in various CO-H₂-H₂O mixtures at 475 °C and different partial pressures of: (a) CO; (b) H₂; (c) H₂O [5].

4.2 Effect of pre-treatment temperature

The relationship between the pre-oxidation temperature and the amount of carbon formed during CO exposure was explained by Gunawardana [1]. Higher oxidation treatment temperature leads to form less surface carbon and lower pre-oxidation temperature leads to form more carbon. Increasing the pre-treatment temperature makes a protective surface oxide layer with better resistance to carbon formation and subsequent metal dusting corrosion.
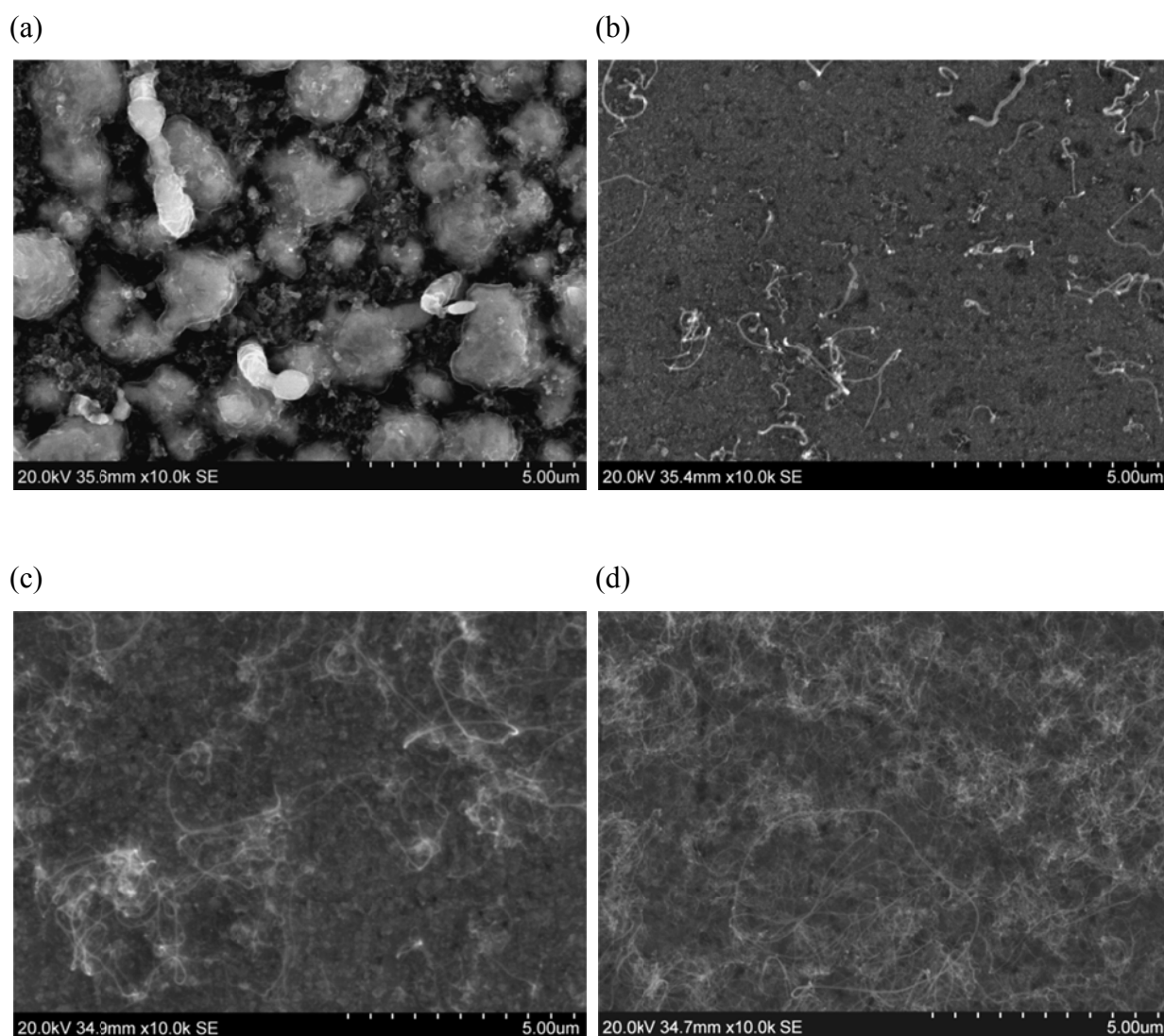
(a)   (b)
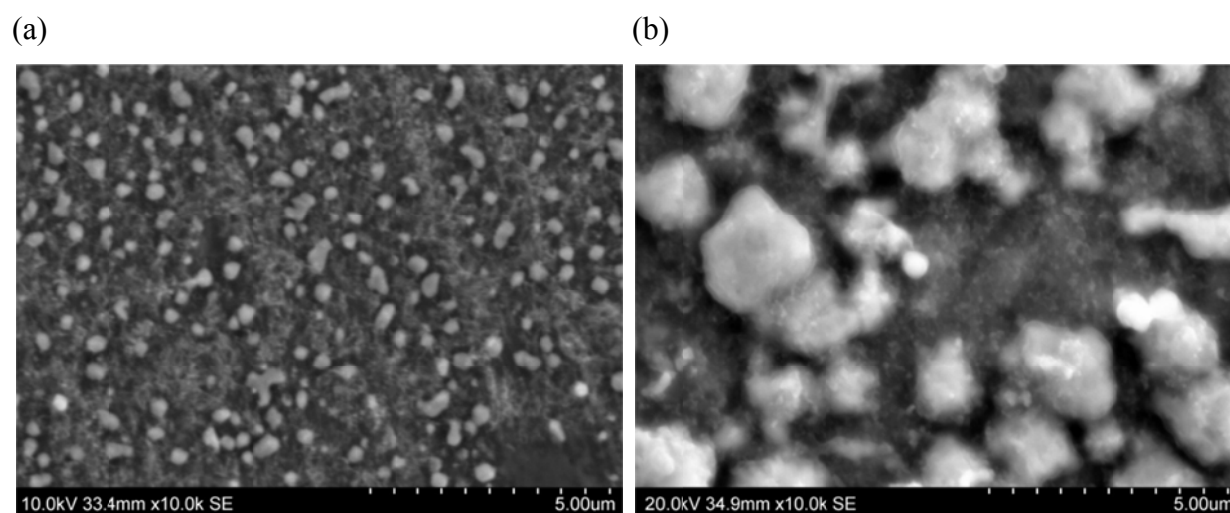
Figure 4.10 SEM micrographs of pre-oxidized (10% steam-Ar gas, 1 bar, 6 h) and CO exposed (10% CO-Ar gas, 650 °C, 1 bar, 1 h) Inconel 601 samples. Oxidation treatment at: (a) 540 °C; (b) 750 °C.

Figure 4.10 compares two samples oxidized at different temperatures. As mentioned in **Chapter 4.1**, crystal-like features on the surface are oxides of Cr with small amount of Ni, Fe and other elements. It is clearly seen in the figure that the higher oxidation treatment temperature forms bigger particles compared to its low temperature counterpart (**Figure 4.10 (b)**).

Cr can diffuse from the bulk to the surface and form an oxide layer at high temperature. When Cr diffuses, grain boundaries provide easy diffusion paths, so it is easy to find the particle agglomeration on the grain boundary (**Figure 4.11**).
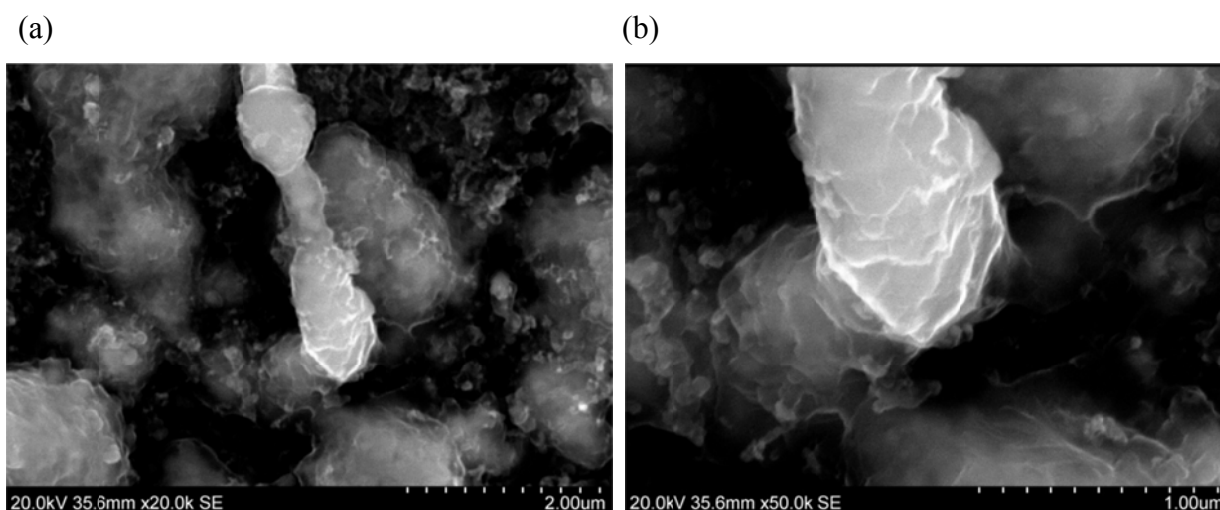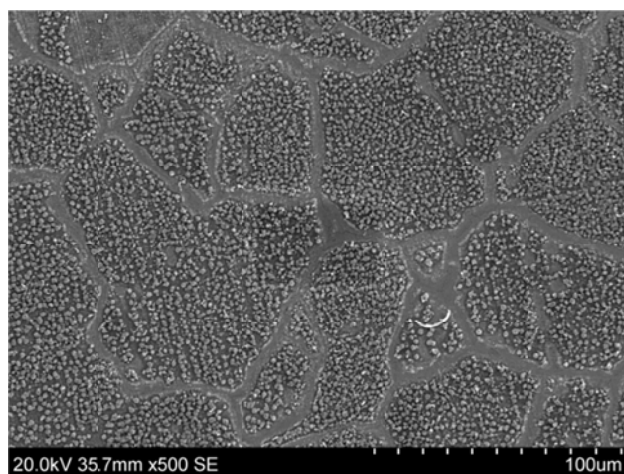

Figure 4.11 SEM micrographs of pre-oxidized (10% steam-Ar gas, 760 °C, 1 bar, 6 h) and CO exposed (10% CO-Ar gas, 650 °C, 1 bar, 1h) Inconel 601 samples.

4.3 Effect of CO exposure temperature

(a)   (b)
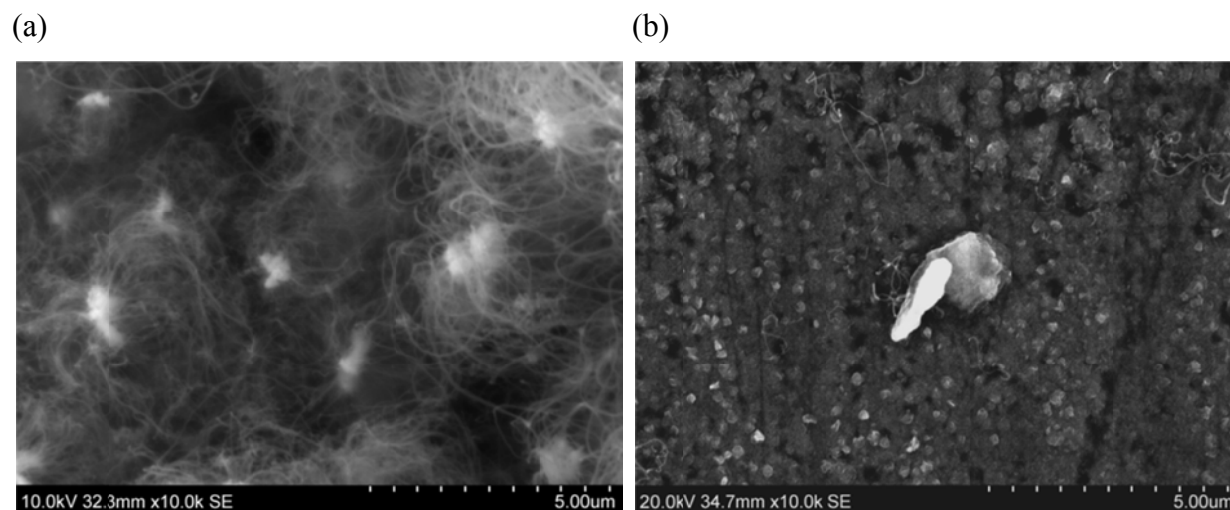
Figure 4.12 SEM micrographs of pre-oxidized (10% steam-Ar gas, 540 °C, 1 bar, 6 h) and CO exposed (10% CO-Ar gas, 1 bar, 20 h) Inconel 601 samples. CO exposed at: (a) 650 °C; (b) 750 °C.

From the **Figure 4.12 (a-b)**, it is evident that lower CO exposure temperature forms more carbon filament. The thickness of the oxide layer is the same since the oxidation treatment is carried out in the same condition. As already mentioned in **Chapter 2**, the thermodynamic potential of carbon formation is high at low temperatures (T < 400 °C) and kinetics is much faster at higher temperatures (T > 800 °C). Since metal dusting is strongly controlled by kinetics, more carbon should be expected at higher temperatures. However, the results show the opposite. Namely there is a lot more carbon on the sample which has been exposed to CO at low temperature (650 °C) compared to its high temperature counterpart (750 °C). This observation is somewhat difficult to explain with the present set of experimental data. But one possible assumption is that the carbon formation is less influenced by the kinetics under these conditions (gas composition, temperature, *etc.*). Gas mixture without H_2 are less affected by kinetics than the gas mixture with H_2 since the Boudouard reaction **(2.3)** is reported to have

slower kinetics than the CO reduction reaction **(2.1)** [6]. Similar trends has been reported by Chun *et al.* that the rate of pitting is higher at 650 °C than 750 °C [21]. However, they used a different gas composition (50% CO – 50% H_2), so it is not correct to compare directly.

5. Conclusion and Further work

5.1 Conclusion

The effects of CO exposure time, pre-treatment temperature and CO exposure treatment temperature on carbon formation were studied in this paper.

Oxidation treatments with polished samples were conducted for 6 h at 540 °C or 760 °C, at 1 bar under 10% steam-Ar gas mixture flowing at a rate of 100 Nml/min. Next, CO exposure treatments with the pre-oxidized sample were carried out at 650 °C or 750 °C, at 1 bar in 100 Nml/min with 10% CO-Ar gas (carbon activity: $a_c \gg 1$) for 1 h to 20 h.

Two characterization methods, optical microscopy and scanning electron microscopy, were used to observe the carbon formation trends on the sample surfaces.

First, the effect of CO exposure time can be summarized by saying that regardless of sample exposure conditions, all samples have more carbon when they are exposed to CO gas for longer time. It becomes more obvious that longer exposure time will produce more carbon filaments by checking SEM micrographs. This can be explained by not only experimental investigations but also the rate expressions **(4.1)** – **(4.8)**. To study the initial stage of metal dusting, samples from when the carbon starts to form on the surface play a key role, because they provide an opportunity to know how the first carbon forms. By checking the oxide layer, whether there are Ni and/or Fe particles or not, the first step of metal dusting can be suggested. Components analysis of the samples is necessary to explain the initial stage of metal dusting.

Second, pre-treatment temperature has an effect in that lower temperature forms more carbon filaments. It is already known from the work by Gunawardana that Cr in bulk can diffuse to the surface at high temperature, and it is also likely that the grain boundaries have provided an

easy diffusion path for Cr.

Third, the effect of CO exposure treatment temperature is that lower temperature (650 °C) forms more carbon filaments than higher temperature (750 °C). However, this trend is not the same as in previous literature where the metal dusting is known as strongly controlled by kinetics. The effect of kinetics on carbon formation might be changed under different conditions (gas composition, temperature, *etc.*). The Boudouard reaction **(2.3)** is reported to have slower kinetics than the CO reduction reaction **(2.1)** [6]. Therefore, when the gas mixture does not contain H_2, the metal dusting is less affected by kinetics than when the gas mixture contains H_2.

5.2 Further work

● Characterization by EDS or by other methods

In **Chapter 4.1**, there were unique features which need to be analyzed further. By analyzing the sample with EDS, composition of the feature will be proved. Also, the samples with very little carbon need to be analyzed to check whether there are Ni and/or Fe particles in the oxide or not. This will help to study initial stage of metal dusting corrosion.

● Analysis of corrosion products

By measuring the weight of corrosion products, the relationship between time and amount of coke can be obtained graphically and quantitatively. It will help to explain the effects of CO exposure time on surface carbon formation.

● Experiments with industrially relevant conditions

Many of industrial plants operate at higher pressure than atmospheric pressure. In addition, various gas mixtures which include hydrogen and oxygen are used. To apply metal dusting corrosion phenomena from the laboratory scale to the industrial scale, experiments under high pressure and relevant gas mixture are needed.

References

1. Gunawardana, P., *Carbon formation phenomena and the initial stage of metal dusting corrosion–an experimental investigation.* Doctoral thesis, Norwegian University of Science and Technology (NTNU), Trondheim, Norway, 2014.
2. Yin, R., *Thermodynamic Roles of Metallic Elements in carburization and Metal dusting.* Oxidation of metals, 2004. **61**(3-4): p. 323-337.
3. Szakálos, P., *Mechanisms of metal dusting.* Doctoral thesis, Royal Institute of Technology (KTH), Stockholm, Sweden, 2004.
4. Bohle, J., et al., *Metal dusting corrosion in steam reforming plants.* Presented at Steam reforming technology user conference, Labuan, Malaysia, 2007.
5. Grabke, H., C. Bracho-Troconis, and E. Müller-Lorenz, *Metal dusting of low alloy steels.* Materials and Corrosion, 1994. **45**(4): p. 215-221.
6. Grabke, H., *Metal dusting.* Materials and corrosion, 2003. **54**(10): p. 736-746.
7. Venvik, H.J., *Metal dusting corrosion initiation in conversion of natural gas to synthesis gas.* Presented at Gas technology conference, Trondheim, Norway, 2011.
8. Albertsen, J.Z., *Experimental and theoretical investigations of metal dusting corrosion in plant exposed nickel-based alloys.* Doctoral thesis, Norwegian University of Science and Technology (NTNU), Trondheim, Norway, 2007.
9. Zeng, K.N.a.Z., *Development of Materials Resistant to Metal Dusting Degradation.* Annual Report, Energy Technology Division, Argonne National Laboratory, 2006.
10. Grabke, H., et al., *Metal dusting of nickel-base alloys.* Materials and Corrosion, 1996. **47**(9): p. 495-504.
11. Amin, A.M.L., *Modeling and Experimental Study of Methane Catalytic Cracking as A Hydrogen Production Technology*. Doctoral thesis, University of Waterloo, Waterloo, Ontario, Canada, 2011.
12. Grabke, H., R. Krajak, and E. Müller-Lorenz, *Metal dusting of high temperature alloys.* Materials and Corrosion, 1993. **44**(3): p. 89-97.
13. Grabke, H., et al., *Effects of grain size, cold working, and surface finish on the metal-dusting resistance of steels.* Oxidation of Metals, 1998. **50**(3-4): p. 241-254.
14. Strauss, S. and H. Grabke, *Role of alloying elements in steels on metal dusting.* Materials and corrosion, 1998. **49**(5): p. 321-327.
15. Grabke, H., *Thermodynamics, mechanisms and kinetics of metal dusting.* Materials and Corrosion, 1998. **49**(5): p. 303-308.
16. Pippel, E., J. Woltersdorf, and R. Schneider, *Micromechanisms of metal dusting on Fe-base and Ni-base alloys.* Materials and corrosion, 1998. **49**(5): p. 309-316.
17. Special Metals, *Product handbook of high-performance nickel alloys.* Retrieved June 23, 2015, from: http://www.specialmetals.com/files/PCC-8064-SM-AlloyHandbook_v04.pdf.
18. *A soap-film burette*. Retrieved June 23, 2015, from: http://www.labunlimited.com/Online-Shop/Chromatography/Flowmeters/Economy-Flowmeter/P0101-0113.html.
19. Dunlap, M. and J. Adaskaveg, *Introduction to the scanning electron microscope.* Theory, practice, & procedures. Facility for Advance Instrumentation. UC Davis, 1997. **52**.

20.   *Comparison of optical microscope (light microscope) and scanning electron microscope*. Retrieved June 23, 2015, from: http://www.ammrf.org.au/myscope/sem/background/#detail.

21.   Chun, C., G. Bhargava, and T. Ramanarayanan, *Metal dusting corrosion of nickel-based alloys.* Journal of the Electrochemical Society, 2007. **154**(5): p. C231-C240.

Appendix A: Risk evaluation

NTNU		Hazardous activity identification process	Prepared by	Number	Date	
			HSE section	HMSRV2601	2011-03-22	
			Approved by	Page	Replaces	
HSE			The Rector		2006-12-01	

Unit: (Department)   *Kjemisk prosessteknologi*   **Date:** 2014-06-19

Line manager: *Edd Blekkan*

Participants in the identification process (incl. function):
(supervisor, student, co-supervisor, others)   Jihye Hwang(Master student), Daham Gunawardana (PhD stipendiat), Hilde Venvik(Supervisor)

Short description of the main activity/main process: Master project for student Jihye Hwang. Project title: Metal dusting.

Is the project work purely theoretical? (YES/NO)   No   *Answer "YES" implies that* **supervisor is assured that no activities**

requiring risk assessment are involved in the work. If YES, briefly describe the activities below. The risk assessment form need not be filled out.

Signatures: *Responsible supervisor:*   *Student:*

ID nr.	Activity/process	Respons-ible person	Existing documentation	Existing safety measures	Laws, regulations etc.	Comment
1	Use of pressurized flamable gases (H2)	Master student: Jihye Hwang		Use required protective equipment: Gas alarms, transportation trolley, safety glasses, gas detector.		Gas bottle pressure: 200-220bar; Operating pressure: 1-25bar; Flamable/explosive gases
2	Use of pressurized poisonous gases (CO)	Master student: Jihye Hwang		Use required protective equipment: Gas alarms, transportation trolley, safety glasses, gas detector.		Gas bottle pressure: 200-220bar; Operating pressure: 1-25bar; poisonous gases
3	Use of pressurized non-toxic/non-flamable gases(CO2, O2, Ar etc.)	Master student: Jihye Hwang		Use required protective equipment: Transportation trolley, safety glasses.		Gas bottle pressure: 200-220bar; Operating pressure: 1-25bar;
4	Use of ethanol/acetone/hexane as cleaning agent	Master student: Jihye Hwang		Use required protective equipment: Safety glasses, gloves.		
5	Leak test and maintainance of setup	Master student: Jihye Hwang		Use required protective equipment: Gas alarms, safety glasses, gas detector, gloves.		Working pressure: 1-25bar; Flamable gases; Poisonous gases;
6	Operating reactor	Master student: Jihye Hwang		Use required protective equipment: Safety glasses, gas detector, gloves.		Pressure, temperature

Appendix

Unit: *(Institute)*   Kjemisk prosessteknologi   **Date:**   2014-06-19

Line manager: *Edd Blekkan*

Participants in the identification process (incl. function):   *Jihye Hwang(Master student), Daham Gunawardana (PhD stipendiat), Hilde Venvik(Supervisor)*
(supervisor, student, co-supervisor, others)

Risk assessment of: Master project for student Jihye Hwang. Project title: Metal dusting.

Signatures: *Responsible supervisor:*   *Student:*

ID nr.	Activity from the identification process form	Potential undesirable incident/strain	Likeli-hood: (1-5)	Consequence: Human (A-E)	Enviroment (A-E)	Economy/ material (A-E)		Risk value (human)	Comments/status Suggested measures
1	Use of pressurized flamable gases (H2)	Small gas leakages/Fire	2	A	A	A		A2	
1	Use of pressurized flamable gases (H2)	Larger gas leakages/Explosion/Fire	1	C	A	C		C1	
2	Use of pressurized poisonous gases (CO)	Small gas leakages/Inhalation	2	B	A	A		B2	
2	Use of pressurized poisonous gases (CO)	Larger gas leakages/Inhalation	1	C	C	C		C1	
3	Use of pressurized non-toxic/non-flamable gases(CO2, O2, Ar etc.)	Gas leakages	2	B	A	A		B2	
4	Use of ethanol/acetone/hexane as cleaning agent	Spills/Chemical exposure	2	A	A	A		A2	
5	Leak test and maintainance of setup	Gas leakages	1	B	A	A		B1	
6	Operating reactor	Uncontrollable warming(overheating)	1	A	A	B		A1	

50

Risk value = Likelihood (1, 2 ...) x consequence (A, B ...). Risk value A1 means very low risk. Risk value E5 means very large and serious risk

Likelihood		Consequence				
Value	Criteria	Grading		Human	Environment	Economy/material
1	**Minimal**: Once every 50 year or less	E	Very critical	May produce fatality/ies	Very prolonged, non-reversible damage	Shutdown of work >1 year.
2	**Low**: Once every 10 years or less	D	Critical	Permanent injury, may produce serious health damage/sickness	Prolonged damage. Long recovery time.	Shutdown of work 0.5-1 year.
3	**Medium**: Once a year or less	C	Dangerous	Serious personal injury	Minor damage. Long recovery time	Shutdown of work < 1 month
4	**High**: Once a month or less	B	Relatively safe	Injury that requires medical treatment	Minor damage. Short recovery time	Shutdown of work < 1week
5	**Very high**: Once a week	A	Safe	Injury that requires first aid	Insignificant damage. Short recovery time	Shutdown of work < 1day

MATRIX FOR RISK ASSESSMENT

CONSEQUENCE					
Very critical	E1	E2	E3	E4	E5
Critical	D1	D2	D3	D4	D5
Dangerous	C1	C2	C3	C4	C5
Relatively safe	B1	B2	B3	B4	B5
Safe	A1	A2	A3	A4	A5
	Minimal	Low	Medium	High	Very high
	LIKELIHOOD				

Explanation of the colors used in the risk matrix.

Color	Description
Red	Unacceptable risk. Safety measures must be implemented.
Yellow	Measures to reduce risk shall be considered.
Green	Acceptabel risk.

Appendix

Appendix B: Flowmeter calibration

Calibration of MFC-1 (H_2)

Date   2014-06-30

Inlet P   26.00 bar

Percent. (%)	9.20	16.20	28.20	40.20	53.20	65.40	79.10	90.50
Flow range (ml)	(0-1)	(0-1)	(1-10)	(1-10)	(1-10)	(10-100)	(10-100)	(10-100)
Volume flowed	1.00	1.00	9.00	9.00	9.00	90.00	90.00	90.00
Readings	2.37	1.28	6.96	4.97	3.78	29.85	24.65	21.44
	2.34	1.34	7.03	5.00	3.75	29.87	24.72	21.41
	2.31	1.31	7.06	5.03	3.75	29.87	24.62	21.44
	2.32	1.32	7.00	4.93	3.79	29.81	24.68	21.47
	2.38	1.28	7.03	4.97	3.78	29.85	24.63	21.38
		1.25	6.97					
Avg. time (s)	2.34	1.30	7.01	4.98	3.77	29.85	24.66	21.43
Avg. time (min)	0.04	0.02	0.12	0.08	0.06	0.50	0.41	0.36
Flowrate (ml/min H2)	**25.60**	**46.27**	**77.05**	**108.43**	**143.24**	**180.90**	**218.98**	**252.01**

$y = 2.7733x - 0.8634$
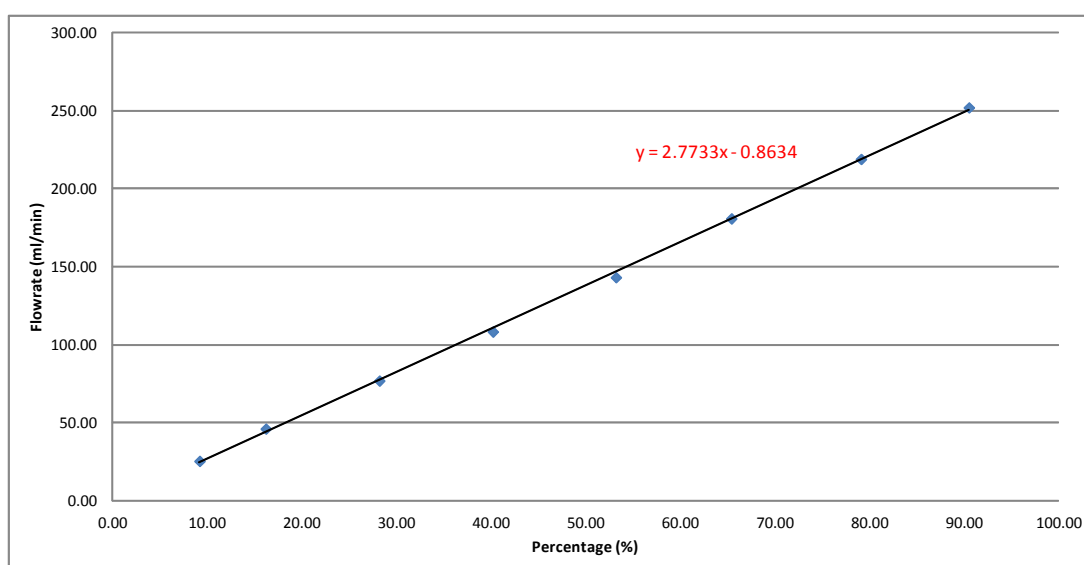
Calibration of MFC-2 (CO_2)

Date   2014-06-26

Inlet P   26.00 bar

Percent. (%)	5.60	16.00	25.90	36.10	46.80	55.70	66.40	76.70	84.30	93.30
Flow range (ml)	(0-1)	(0-1)	(0-1)	(0-1)	(1-10)	(1-10)	(1-10)	(1-10)	(1-10)	(1-10)
Volume flowed	1.00	1.00	1.00	1.00	9.00	9.00	9.00	9.00	9.00	9.00
Readings	12.06	3.87	2.47	1.78	12.25	10.37	8.50	7.25	6.38	5.59
	11.97	3.84	2.46	1.71	12.25	10.34	8.56	7.22	6.32	5.50
	12.03	3.88	2.50	1.75	12.22	10.41	8.56	7.25	6.41	5.54
	12.03	3.84	2.44	1.79	12.19	10.41	8.53	7.29	6.35	5.56
	11.97	3.84	2.44	1.72	12.25	10.35	8.56	7.28	6.34	5.56
Avg. time (s)	12.01	3.85	2.46	1.75	12.23	10.38	8.54	7.26	6.36	5.55
Avg. time (min)	0.20	0.06	0.04	0.03	0.20	0.17	0.14	0.12	0.11	0.09
Flowrate (ml/min CO2)	**5.00**	**15.57**	**24.37**	**34.29**	**44.15**	**52.04**	**63.22**	**74.40**	**84.91**	**97.30**

$y = 1.0225x - 2.2974$
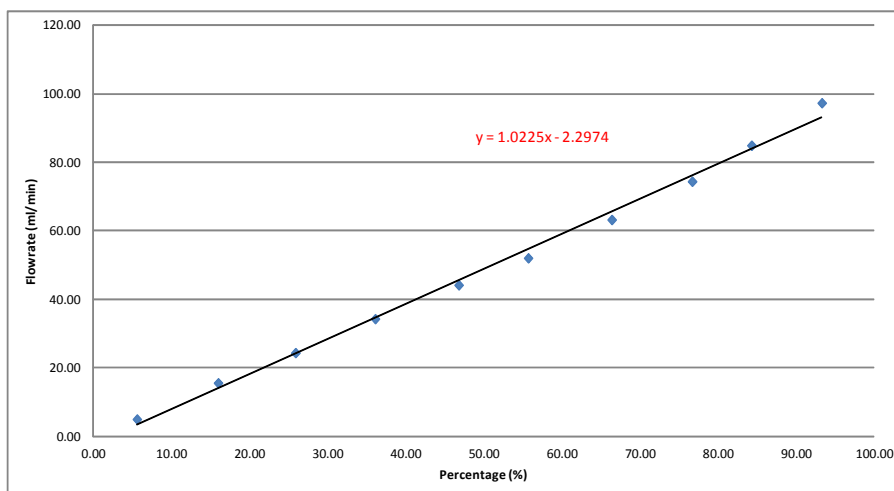
Calibration of MFC-2 (0.5%O$_2$/Ar synthesizes gas)

Date   2014-06-26

Inlet P   26.00 bar

Percent. (%)	5.70	14.60	24.10	34.60	42.50	54.50	64.20	75.20	84.50	93.10
Flow range (ml)	(0-1)	(0-1)	(1-10)	(1-10)	(1-10)	(1-10)	(1-10)	(10-100)	(10-100)	(10-100)
Volume flowed	1.00	1.00	9.00	9.00	9.00	9.00	9.00	90.00	90.00	90.00
Readings	5.30	2.00	10.75	7.72	6.31	5.03	4.25	35.81	31.66	28.66
	4.97	1.97	10.75	7.69	6.35	5.06	4.25	35.78	31.69	28.62
	5.00	2.03	10.72	7.71	6.35	5.04	4.25	35.78	31.69	28.59
	4.97	2.03	10.78	7.75	6.34	5.06	4.32	35.84	31.69	28.66
	4.97	2.03	10.78	7.69	6.34	5.04	4.28	35.81	31.72	28.63
Avg. time (s)	5.04	2.01	10.76	7.71	6.34	5.05	4.27	35.80	31.69	28.63
Avg. time (min)	0.08	0.03	0.18	0.13	0.11	0.08	0.07	0.60	0.53	0.48
Flowrate (ml/min 0.5%O2)	**11.90**	**29.82**	**50.20**	**70.02**	**85.20**	**107.02**	**126.46**	**150.82**	**170.40**	**188.60**

$y = 2.0023x + 0.3296$
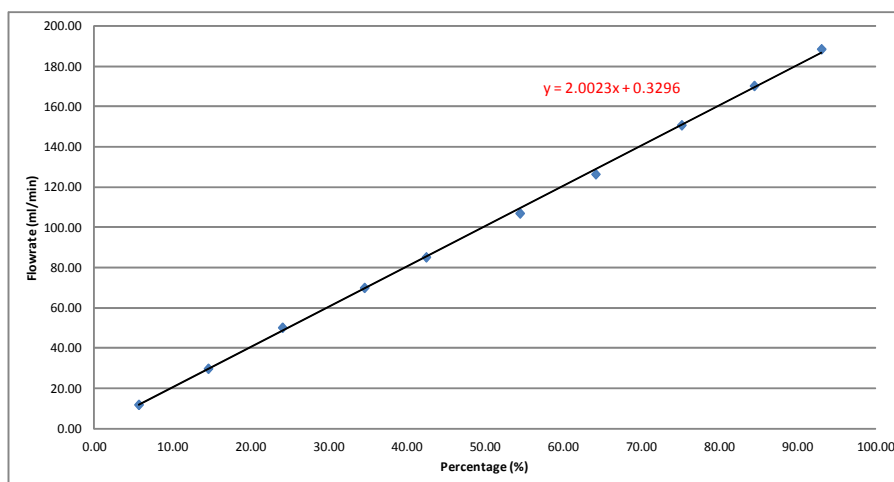
Calibration of MFC-3 (CO)

Date   2014-06-30
Inlet P   26.00 bar

Percent. (%)	5.50	14.70	24.50	34.30	44.20	53.20	64.70	74.10	82.80	92.30
Flow range (ml)	(0-1)	(1-10)	(1-10)	(1-10)	(1-10)	(10-100)	(10-100)	(10-100)	(10-100)	(10-100)
Volume flowed	1.00	9.00	9.00	9.00	9.00	90.00	90.00	90.00	90.00	90.00
Readings	3.38	12.44	7.69	5.65	4.44	35.97	29.78	26.07	23.28	20.88
	3.40	12.41	7.69	5.59	4.38	36.09	29.72	26.07	23.31	20.75
	3.34	12.47	7.69	5.66	4.41	36.03	29.75	26.09	23.34	20.88
	3.40	12.41	7.72	5.66	4.46	35.97	29.78	26.04	23.34	20.87
	3.34	12.44	7.72	5.69	4.37	35.96	29.72	26.00	23.35	20.85
	3.37		7.75	5.56	4.47	35.94				20.88
			7.75	5.69						
			7.75							
Avg. time (s)	3.37	12.43	7.72	5.64	4.42	35.99	29.75	26.05	23.32	20.85
Avg. time (min)	0.06	0.21	0.13	0.09	0.07	0.60	0.50	0.43	0.39	0.35
Flowrate (ml/min CO)	**17.80**	**43.43**	**69.95**	**95.70**	**122.13**	**150.03**	**181.51**	**207.26**	**231.52**	**258.97**

$y = 2.7763x + 1.7083$
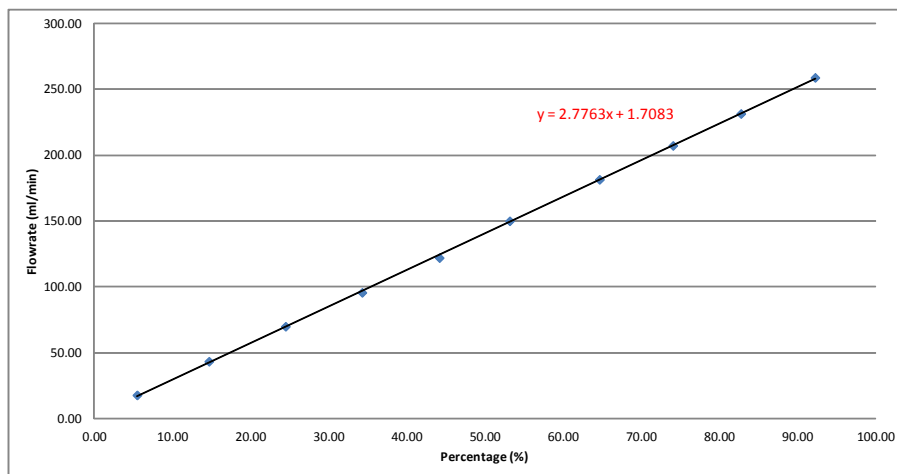
Calibration of MFC-3 (O$_2$)

Date   2014-06-30

Inlet P   26.00 bar

Percent. (%)	4.60	13.90	24.50	34.00	43.90	54.00	64.10	73.80	84.40	92.80
Flow range (ml)	(0-1)	(0-1)	(1-10)	(1-10)	(1-10)	(10-100)	(10-100)	(10-100)	(10-100)	(10-100)
Volume flowed	1.00	1.00	9.00	9.00	9.00	90.00	90.00	90.00	90.00	90.00
Readings	3.90	1.47	7.72	5.72	4.41	35.78	30.37	26.56	23.18	21.07
	3.91	1.50	7.75	5.72	4.43	35.84	30.38	26.53	23.22	21.06
	3.94	1.44	7.72	5.65	4.47	35.84	30.44	26.53	23.18	21.00
	3.93	1.43	7.78	5.68	4.47	35.87	30.37	26.50	23.16	21.03
	3.94	1.43	7.78	5.69	4.44	35.78	30.41	26.47	23.16	21.06
	4.00	1.44	7.85	5.62			30.38			
	4.00	1.50		5.62						
Avg. time (s)	3.95	1.46	7.77	5.67	4.44	35.82	30.39	26.52	23.18	21.04
Avg. time (min)	0.07	0.02	0.13	0.09	0.07	0.60	0.51	0.44	0.39	0.35
Flowrate (ml/min O2)	**15.21**	**41.14**	**69.53**	**95.21**	**121.51**	**150.75**	**177.68**	**203.64**	**232.96**	**256.61**

$y = 2.7306x + 2.6211$
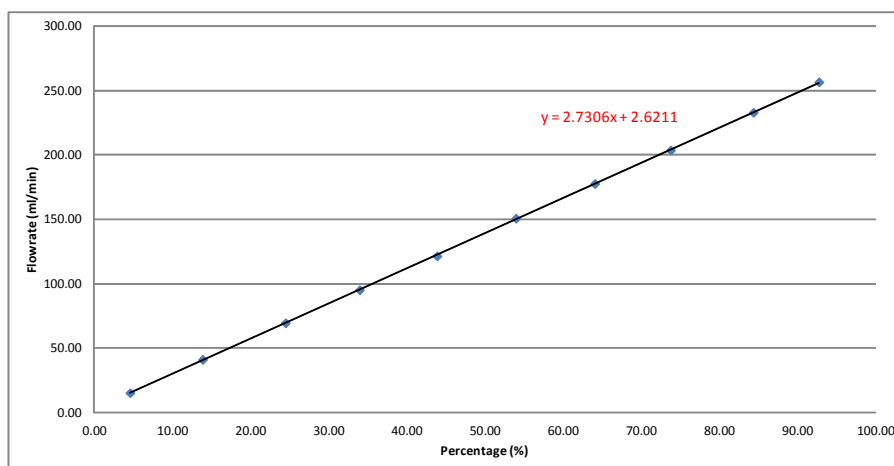
Calibration of MFC-5 (Ar)

Date   2014-06-25

Inlet P   26.00 bar

Percent. (%)	6.80	15.60	24.80	35.40	45.20	54.20	68.70	82.30	91.30
Flow range (ml)	(0-1)	(0-1)	(0-1)	(1-10)	(1-10)	(10-100)	(10-100)	(10-100)	(10-100)
Volume flowed	1.00	1.00	1.00	9.00	9.00	90.00	90.00	90.00	90.00
Readings	3.44	1.75	1.12	7.19	5.66	46.31	37.00	30.75	27.40
	3.41	1.75	1.06	7.10	5.63	46.28	37.09	30.75	27.50
	3.44	1.75	1.09	7.16	5.69	46.18	36.96	30.63	27.50
	3.40	1.72	1.12	7.19	5.65	46.22	36.90	30.72	27.47
	3.43	1.72	1.09	7.13	5.63	46.22	36.96	30.72	27.41
Avg. time (s)	3.42	1.74	1.10	7.15	5.65	46.24	36.98	30.71	27.46
Avg. time (min)	0.06	0.03	0.02	0.12	0.09	0.77	0.62	0.51	0.46
Flowrate (ml/min Ar)	17.52	34.52	54.74	75.48	95.54	116.78	146.02	175.82	196.68

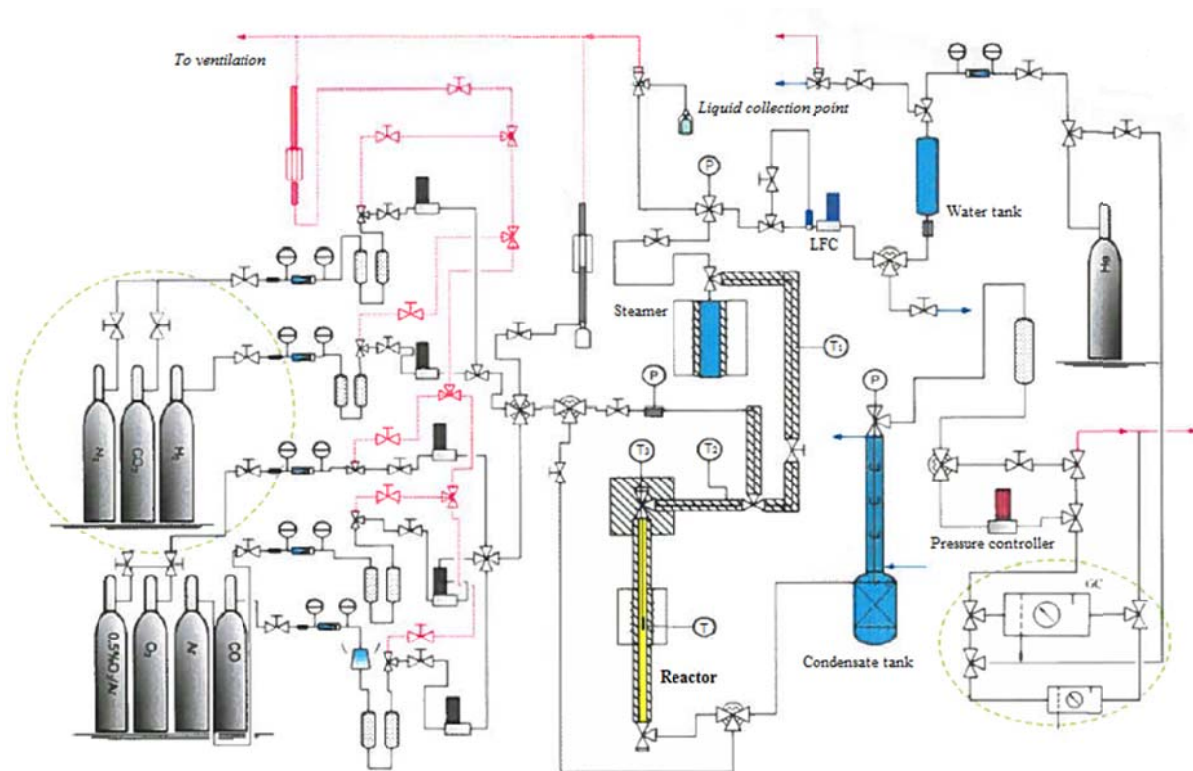$y = 2.1174x + 1.6308$
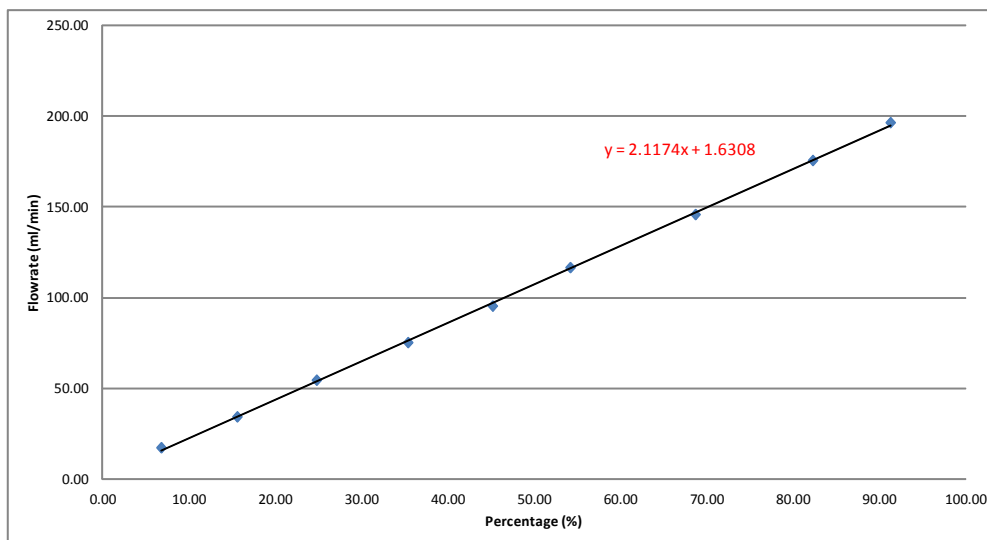
Appendix C: Setup details

Figure C.1 Schematic diagram of setup [1]

Mass flow controller: Bronkhorst HI-TEK mass flow controller

Liquid flow controller: Bronkhorst HI-TEK liquid flow controller

Pressure controller: Bronkhorst EL-PRESS electronic pressure controller

Controller box: Bronkhorst controller-readout boxes

Temperature controller: Eurotherm 2416 controller

Appendix